

# THE MASSIVE SURVEY – I. A VOLUME-LIMITED INTEGRAL-FIELD SPECTROSCOPIC STUDY OF THE MOST MASSIVE EARLY-TYPE GALAXIES WITHIN 108 MPC

CHUNG-PEI MA<sup>1</sup>, JENNY E. GREENE<sup>2</sup>, NICHOLAS MCCONNELL<sup>3</sup>, RYAN JANISH<sup>4</sup>, JOHN P. BLAKESLEE<sup>5</sup>, JENS THOMAS<sup>6</sup> AND JEREMY D. MURPHY<sup>2</sup>

<sup>1</sup> Department of Astronomy, University of California, Berkeley, CA 94720, USA; cpma@berkeley.edu

<sup>2</sup> Department of Astrophysical Sciences, Princeton University, Princeton, NJ 08544, USA

<sup>3</sup> Institute for Astronomy, University of Hawaii at Manoa, Honolulu, HI 96822, USA

<sup>4</sup> Department of Physics, University of California, Berkeley, CA 94720, USA

<sup>5</sup> Dominion Astrophysical Observatory, NRC Herzberg Institute of Astrophysics, Victoria, BC V9E 2E7, Canada

<sup>6</sup> Max Planck-Institute for Extraterrestrial Physics, Giessenbachstr. 1, D-85741 Garching, Germany

*Draft version October 14, 2014*

## ABSTRACT

Massive early-type galaxies represent the modern-day remnants of the earliest major star formation episodes in the history of the universe. These galaxies are central to our understanding of the evolution of cosmic structure, stellar populations, and supermassive black holes, but the details of their complex formation histories remain uncertain. To address this situation, we have initiated the MASSIVE Survey, a volume-limited, multi-wavelength, integral-field spectroscopic (IFS) and photometric survey of the structure and dynamics of the  $\sim 100$  most massive early-type galaxies within a distance of 108 Mpc. This survey probes a stellar mass range  $M^* \gtrsim 10^{11.5} M_{\odot}$  and diverse galaxy environments that have not been systematically studied to date. Our wide-field IFS data cover about two effective radii of individual galaxies, and for a subset of them, we are acquiring additional IFS observations on sub-arcsecond scales with adaptive optics. We are also acquiring deep  $K$ -band imaging to trace the extended halos of the galaxies and measure accurate total magnitudes. Dynamical orbit modeling of the combined data will allow us to simultaneously determine the stellar, black hole, and dark matter halo masses. The primary goals of the project are to constrain the black hole scaling relations at high masses, investigate systematically the stellar initial mass function and dark matter distribution in massive galaxies, and probe the late-time assembly of ellipticals through stellar population and kinematical gradients. In this paper, we describe the MASSIVE sample selection, discuss the distinct demographics and structural and environmental properties of the selected galaxies, and provide an overview of our basic observational program, science goals and early survey results.

*Subject headings:* galaxies: elliptical and lenticular, cD — galaxies: evolution — galaxies: kinematics and dynamics — galaxies: stellar content — galaxies: structure — dark matter

## 1. INTRODUCTION

The most massive early-type galaxies in the local universe are powerful probes of galaxy evolution. They formed most of their stars rapidly at redshifts  $z > 2$  (e.g., Blakeslee et al. 2003; Thomas et al. 2005) but have grown in number and size by a factor of two or more since  $z \approx 1$  (e.g., Daddi et al. 2005; Trujillo et al. 2006; Faber et al. 2007; van der Wel et al. 2008; Damjanov et al. 2009; Cappellari et al. 2009; van Dokkum et al. 2010; van de Sande et al. 2011), probably in large part through dissipationless merging and accretion (e.g., De Lucia et al. 2006; Boylan-Kolchin et al. 2006; Naab et al. 2009; Kormendy & Bender 2009; Oser et al. 2010; Thomas et al. 2014). They contain nuclear black holes whose masses  $M_{\text{BH}}$  are correlated with properties of the stellar bulge (e.g., Magorrian et al. 1998; Ferrarese & Merritt 2000; Gebhardt et al. 2000; Tremaine et al. 2002; Marconi & Hunt 2003; Häring & Rix 2004; Gültekin et al. 2009; Beifiori et al. 2012; McConnell & Ma 2013; Kormendy & Ho 2013). These scaling relations between black holes and their host galaxies imply co-evolution between the two components over the lifetime of a galaxy, but the detailed mechanisms remain uncertain.

Integral field spectroscopy (IFS) over a wide radial

range provides an effective tool to study the spatial and kinematic structure, star formation histories, and stellar and dark matter halo masses of local galaxies. While many IFS surveys are ongoing, such as VENGA/VIXENS (Blanc et al. 2013), CALIFA (Sánchez et al. 2012), SLUGGS (Brodie et al. 2014), and eventually MaNGA (Bundy et al. in preparation) and SAMI (Croom et al. 2012), none of them probes the volume, mass range, or spatial scales required to systematically study the most massive elliptical galaxies, a regime that is critical for understanding the assembly of galaxies and supermassive black holes. The ATLAS<sup>3D</sup> project (Cappellari et al. 2011) surveyed 260 galaxies within 42 Mpc. Because of their relatively small survey volume, only a handful of galaxies had stellar masses  $M^* \gtrsim 10^{11.5} M_{\odot}$ . Their field-of-view of  $33'' \times 41''$  provided coverage within one half-light radius of most of their sample galaxies.

In this paper we describe MASSIVE, a volume-limited, multi-wavelength, spectroscopic and photometric survey of the most massive galaxies in the local universe. The sample includes 116 candidate galaxies in the northern sky with distance  $D < 108$  Mpc and absolute  $K$ -band magnitude  $M_K < -25.3$ , corresponding to stellar masses  $M^* \gtrsim 10^{11.5} M_{\odot}$ . MASSIVE is designed to address a wide range of outstanding problems in elliptical galaxy

formation, including the variation in dark matter fraction and stellar initial mass function (IMF) within and among early-type galaxies, the connection between black hole accretion and galaxy growth, and the late-time assembly of galaxy outskirts. We combine comprehensive ground-based NIR imaging with IFS data to measure stellar populations and kinematics out to  $\sim 2$  effective radii. Using the Mitchell Spectrograph (formerly called VIRUS-P; Hill et al. 2008) at McDonald Observatory, we cover a  $107'' \times 107''$  field of view with  $4''$  fibers. Thus, we are sensitive to low surface-brightness emission in the outer parts of the galaxies (e.g., Murphy et al. 2011; Adams et al. 2012; Greene et al. 2012).

For a subset of galaxies, we are obtaining additional adaptive-optics assisted IFS data to map the stellar kinematics on  $\sim 100$  pc scales, within the sphere of influence of nuclear black holes. The high-resolution data are required to detect the gravitational effect of the supermassive black holes on the stellar orbits. These data alone, however, are insufficient for removing the degeneracy among the dark matter halo, the stellar mass-to-light ratio, and the central black hole mass (Gebhardt & Thomas 2009). We therefore combine the high-resolution and wide-field IFS data for simultaneous modelling of the three mass components (e.g., Schulze & Gebhardt 2011; McConnell et al. 2011a,b, 2012; Rusli et al. 2013b; Thomas et al. 2014).

We are also acquiring deep  $K$ -band data at UKIRT and CFHT to measure the extended stellar halos of these luminous galaxies and determine more accurately their  $K$ -band magnitudes.

The wide-field IFU portion of the survey is currently complete at  $M_K < -25.7$  and 75% complete at  $M_K < -25.5$ . Seven galaxies in the survey have published values of black hole mass (Sec 3.6); 15 additional galaxies have existing or incoming high-resolution kinematic data. Deep  $K$ -band photometry has been obtained for 45 galaxies thus far.

The selection of the galaxy sample for the MASSIVE survey is described in Section 2. Since this survey is volume-limited and defined by the stellar masses of the galaxies via their  $K$ -band luminosities, we discuss in detail the determinations of distance and absolute  $K$ -band magnitude. Basic properties of the survey galaxies such as stellar mass, size, velocity dispersion, shape, color, and central black holes are presented in Section 3. We illustrate the distinct demographics of these galaxies and compare their locations in parameter space with lower-mass early type galaxies. In Section 4, we investigate the larger-scale environments of these massive galaxies using three 2MASS-selected galaxy group catalogs within the local volume. Our observing strategies with large-format IFS, AO-assisted IFS, and deep  $K$ -band imaging are discussed in Section 5. Sample spectra from the Mitchell IFS and kinematic maps of NGC 1600 are shown. We discuss the primary science goals of the survey and present early science results in Section 6.

Appendix A tabulates the 116 candidate galaxies in the MASSIVE survey and their key physical properties. Appendix B provides a montage of the 78 MASSIVE galaxies with SDSS photometry.

We assume  $H_0 = 70 \text{ km s}^{-1} \text{ Mpc}^{-1}$  throughout the paper.

TABLE 1  
SELECTION CRITERIA FOR MASSIVE GALAXIES

Distance	$D < 108 \text{ Mpc}$
Absolute $K$ magnitude	$M_K < -25.3$
Declination	$\delta > -6^\circ$
Galactic extinction	$A_V < 0.6$
Morphology	E and S0

## 2. SAMPLE SELECTION

### 2.1. Overview

The main selection criteria of our survey are summarized in Table 1. The survey volume of radius  $D < 108$  Mpc is chosen to be large enough to encompass the Coma cluster. This volume is more than an order of magnitude larger than that probed by ATLAS<sup>3D</sup>, enabling us to obtain a statistical sample of early-type galaxies at the highest end of the galaxy mass function. The corresponding redshift limit is  $cz < 7560 \text{ km s}^{-1}$  or  $z < 0.025$  (for  $H_0 = 70 \text{ km s}^{-1} \text{ Mpc}^{-1}$ ).

Within the survey volume, our goal is to select galaxies above a given total stellar mass. Since selection based on  $K$ -band luminosities is close to a stellar mass selection, particularly for these red galaxies, we use the near-infrared  $K$ -band magnitude from the Extended Source Catalog (XSC; Jarrett et al. 2000) of the Two Micron All Sky Survey (2MASS; Skrutskie et al. 2006). This catalog contains photometric measurements in the  $J$ ,  $H$ , and  $K$  bands of  $\sim 1.6 \times 10^6$  objects with  $K \leq 13.5$  mag. The data have a mean photometric accuracy better than 0.1 mag and are mostly unaffected by interstellar extinction and stellar confusion, although the 2MASS luminosities may be systematically underestimated for very extended objects (see Sec 2.3).

Peculiar velocities add uncertainties to the determination of distances and absolute magnitudes, and consequently the selection of our sample. We use the 2MASS Galaxy Redshift Survey (2MRS; Huchra et al. 2012) and the group catalog based on 2MRS (Crook et al. 2007) to correct the radial velocity-derived distances. We begin with an initial velocity cutoff corresponding to a redshift-distance of 140 Mpc and  $M_K < -22$  and correct for peculiar velocities for galaxies in the 2MRS group catalog (see Sec 2.2). We then select those galaxies with  $D < 108$  Mpc,  $M_K < -25.3$  mag, declination  $\delta > -6^\circ$ , and galactic extinction  $A_V < 0.6$ .

Finally, we restrict our sample to galaxies classified as elliptical or S0 in the HyperLeda database<sup>1</sup> (Paturel et al. 2003). We remove 14 galaxies from the sample because their photometry is compromised by either a foreground star or a companion galaxy, and the stellar mass is likely to be overestimated (see Sec 2.5). We do not remove any galaxies based on their size on the sky; in practice, most galaxies in the survey have effective radii larger than  $10''$  (listed in Table 3; see discussion in Sec 3.2) and are therefore well-resolved by the  $4''$  fibers of the Mitchell Spectrograph.

This set of selection criteria results in 116 candidate galaxies listed in Table 3. Among these, 72 galaxies have

<sup>1</sup> <http://leda.univ-lyon1.fr>

$M_K < -25.5$  and  $D < 105$  Mpc and are our high priority targets. We are obtaining deeper  $K$ -band imaging to improve on the relatively shallow photometry provided by 2MASS. The more robust measurements of the total  $K$ -band magnitude for our candidate galaxies will help alleviate the uncertainties near the magnitude and distance cutoffs and sharpen the survey boundaries and the final sample size.

Below we describe the key selection criteria in more detail.

### 2.2. Distance

We need accurate distance estimates to determine the absolute  $K$ -band magnitudes, the volume cutoff, and the measurements of  $M_{\text{BH}}$  and  $M^*$ . Only 9 galaxies in our survey have existing distances measured from the surface-brightness fluctuation (SBF) method (e.g., Blakeslee et al. 2009, 2010) for either the individual galaxies or the groups in which they reside. Among these, three are in the Virgo cluster (NGC 4472, 4486, 4649) at 16.7 Mpc (Blakeslee et al. 2009), four are in the Coma cluster (NGC 4816, 4839, 4874, 4889) at 102.0 Mpc (Blakeslee 2013), and two are in the Perseus group (NGC 7619 and 7626) at 54.0 Mpc (Cantiello et al. 2007). We adopt SBF distances for these 9 galaxies.

For the rest of the sample, we assign the distance in one of two ways, depending on whether or not a galaxy is identified as belonging to a group. For galaxies in groups, we correct for local peculiar velocities using group-corrected redshift distances; for galaxies not in groups, we use redshift distances based on radial velocities corrected with a flow model, as described below.

To determine group membership, we use the catalog of galaxy groups constructed from the friends-of-friends (FOF) algorithm applied to 2MRS (Crook et al. 2007). The 2MRS contains follow-up spectroscopic data and redshifts for a subset of 43,533 galaxies in 2MASS. It is 97.6% complete down to  $K = 11.75$  mag over 91% of the sky. The median uncertainty in the radial velocities for galaxies with absorption-line spectra is 29 and 41 km s<sup>-1</sup>, respectively, for the two main spectrographs used in the survey. Crook et al. (2007) present a catalog of galaxy groups using the 2MRS redshifts. It is complete to a limiting radial velocity of 10<sup>4</sup> km s<sup>-1</sup>. The high-density-contrast (HDC) catalog in this work provides galaxy membership in groups that have a density contrast of 80 or more, corresponding to FOF linking parameters of 0.93 Mpc (for  $h = 0.7$ ) in the transverse directions and 350 km s<sup>-1</sup> along the line of sight.

For galaxies that reside in HDC groups with three or more members, we use the mean group distance from the HDC catalog, converted from  $H_0 = 73$  km s<sup>-1</sup> Mpc<sup>-1</sup> to our adopted value of 70 km s<sup>-1</sup> Mpc<sup>-1</sup>. The group distance is determined using velocities from the flow model of Mould et al. (2000) to account for the most obvious local distortions and large-scale flows. The model first converts from the heliocentric frame to the Local Group frame, and then adjusts the redshift-inferred distances of galaxies near the Virgo Cluster, Shapley Supercluster, and the Great Attractor region.<sup>2</sup> Then, the Local

<sup>2</sup> However, we use the SBF distance for the Virgo galaxies, and none of our galaxies are in Shapley or the Great Attractor regions, as these are in the southern sky.

Group frame velocities for all galaxies are corrected for the estimated gravitational pull of the Virgo, the Great Attractor, and Shapley mass concentrations.

For galaxies not residing in any HDC group, we assign the distances using velocities from the same flow model (as provided by NED and converted to our  $H_0$ ) to ensure that the distances for group and field galaxies in our survey are computed in the same rest frame.

While we have used the best available distance measurements (listed in Table 3), uncertainties will unavoidably cause a small fraction of the galaxies near our mass and distance cutoffs to move into and out of the sample. We have attempted to quantify the outstanding distance uncertainties by comparing our adopted distances with the redshift-independent distances tabulated by NED for 39 objects in our sample. We find the mean offset to be 1.5 Mpc, but  $\sim 20\%$  of the cases differ by  $> 10$  Mpc. Since galaxy populations over a few tens of Mpc or a few tenths of a magnitude are not expected to change, we do not anticipate the uncertainty in the exact membership near our survey boundaries to impact our results. Our dynamical measurements of  $M_{\text{BH}}$  and  $M^*$ , however, do depend on the distance linearly, and all current such measurements are affected by this uncertainty. Significant improvements can be achieved with more SBF data with the *Hubble Space Telescope*.

### 2.3. $K$ -band magnitude

The 2MASS XSC database provides a variety of magnitude measurements for each extended source in the  $J$ ,  $H$ , and  $K$  bands. To determine each galaxy’s absolute  $K$ -band luminosity, we begin with the “total” extrapolated  $K$ -band magnitude (XSC parameter `k_m_ext`), which is measured in an aperture consisting of the isophotal aperture plus the extrapolation of the surface brightness profile based on a single Sérsic fit to the inner profile (Jarrett et al. 2003). We compute the absolute  $K$ -band magnitudes using

$$M_K = K - 5 \log_{10} D - 25 - 0.11 A_V, \quad (1)$$

where  $K$  is given by `k_m_ext`, and  $D$  is the distance in Mpc described in Sec 2.2. We use galactic extinction  $A_V$  (Landolt  $V$ ) from Schlafly & Finkbeiner (2011) and the reddening relation of Fitzpatrick (1999) with  $R_V = A_V/E_{B-V} = 3.1$ . The values of  $K$ ,  $A_V$ , and  $M_K$  for all galaxies are listed in Table 3. These  $K$ -band magnitudes form the basis for our selection and are used to estimate stellar masses (§ 3.1).

The relatively shallow photometry provided by 2MASS XSC (the  $1\text{-}\sigma$  sky noise in  $K$  is 20.0 mag arcsec<sup>-2</sup>) has led to some concerns that the  $K$ -band luminosities of massive galaxies are underestimated by 2MASS (e.g., Lauer et al. 2007b; Schombert & Smith 2012; Kormendy & Ho 2013). When the radial range is too small to provide an accurate Sérsic index for the light profiles of early-type galaxies, their total luminosities can be particularly biased low.

To assess the impact of potential biases in 2MASS  $K$ -band magnitudes on our galaxy selection, we examine the sample of 219 early-type galaxies targeted for an HST imaging study in Lauer et al. (2007b). We use  $V - K = 2.98$  (Kormendy & Ho 2013) to transform the  $V$ -band luminosities (largely based on the RC3 Catalog)

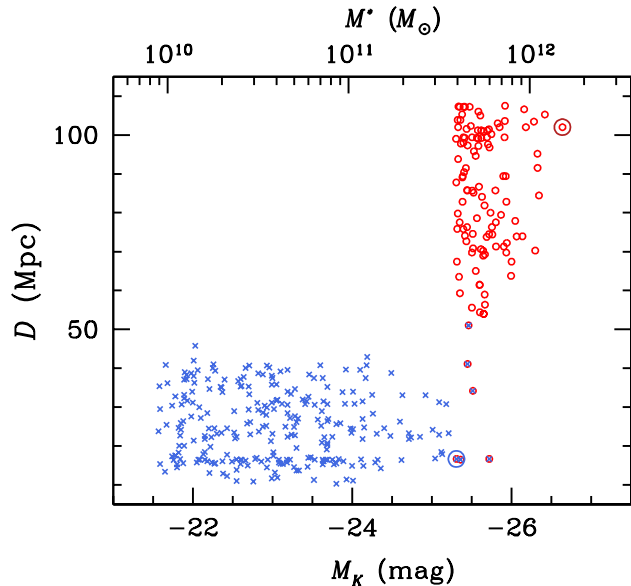


FIG. 1.— Distance and absolute  $K$ -band magnitude of galaxies in the MASSIVE survey (red circles) and ATLAS<sup>3D</sup> survey (blue crosses). Stellar masses estimated from Equation (2) are also shown. Only 6 galaxies in ATLAS<sup>3D</sup> are luminous enough to pass our  $K$ -band magnitude cut. The rest of our sample all lie beyond the volume limit of 42 Mpc surveyed by ATLAS<sup>3D</sup>. The big circles indicate NGC 4889 (red) and M87 (blue).

in their sample to the  $K$ -band. A total of 31 galaxies in this sample lie within our survey volume of  $D < 108$  Mpc and above the luminosity cut of  $M_K = -25.3$  mag; among these, 18 have  $\delta > -6^\circ$  and would belong to our survey if the deeper  $V$ -band photometry and  $V - K$  relation were used to select bright galaxies.<sup>3</sup> We find all 18 to be in our MASSIVE sample; our  $K$ -band selection therefore does not appear to be much affected by potential systematic underestimates in the 2MASS  $K$ -band magnitude according to this test.

We are acquiring deep wide-field  $K$ -band photometry (Sec 5.3) for more robust measurements of the total magnitude for the galaxies in our sample. M87, for instance, has  $M_K = -25.31$  mag according to the 2MASS XSC and is only slightly above our magnitude cut. Analysis of deeper photometric data, however, finds  $M_K = -26.08$  mag, a factor of two more luminous (Läscher et al. 2014). Although M87 is likely to be a worst case because of its angular extent on the sky, this large discrepancy underscores the need for deeper  $K$ -band imaging data. Our dataset will also reduce the uncertainties near our magnitude and distance cutoffs and help refine the final sample selection for IFS observations.

#### 2.4. Parameter Space

Figure 1 highlights the distinct parameter space in distance and stellar mass occupied by MASSIVE galaxies. Only 6 galaxies in this survey were included in

<sup>3</sup> We exclude IC 1565, which is at a distance of  $\sim 150$  Mpc according to NED; it is incorrectly listed as 38.2 Mpc in Lauer et al. (2007b).

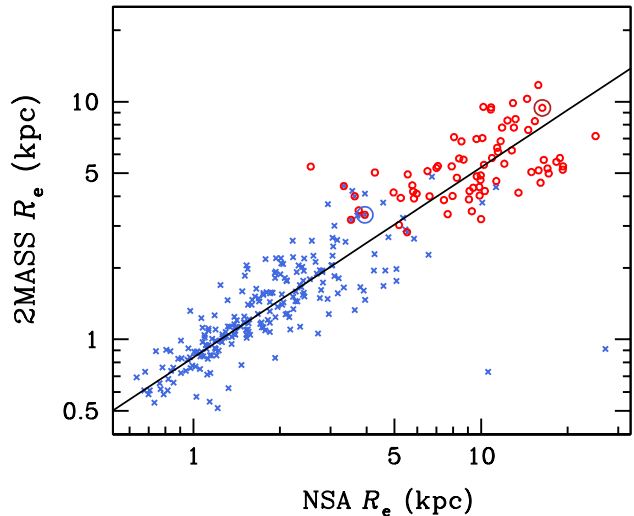


FIG. 2.— Comparison of infrared (from 2MASS) and optical (from NSA) galaxy sizes for the MASSIVE (red circles) and ATLAS<sup>3D</sup> (blue crosses) surveys. 77 galaxies in the MASSIVE sample are listed in the NSA. The 2MASS  $R_e$  is systematically lower than the NSA values. The best-fit relation (black line) is given in Equation (4). The big circles indicate NGC 4889 (red) and M87 (blue).

ATLAS<sup>3D</sup>; three are in the Virgo Cluster: NGC 4486 (M87), NGC 4472 (M49), NGC 4649 (M60); the others are NGC 5322, NGC 5353, and NGC 5557. The larger survey volume (by more than a factor of 15) allows us to sample the galaxy mass function at  $M^* \gtrsim 10^{11.5} M_\odot$ .

The ongoing CALIFA survey will target  $\sim 600$  diameter-selected local galaxies with major axes between  $45''$  and  $80''$  (in the SDSS  $r$ -band) and a redshift range of  $0.005 < z < 0.03$ . About  $1/3$  of the galaxies are expected to be bulge-dominated (Sánchez et al. 2012). Despite the selection on galaxy sizes, the CALIFA sample is shown to be representative of galaxies with  $10^{9.7} < M^* < 10^{11.44} M_\odot$  (Walcher et al. 2014), complementary to our mass selection of  $M^* \gtrsim 10^{11.5} M_\odot$ .

#### 2.5. Skipped Targets

A total of 14 galaxies pass our selection criteria but are in the field of view of a bright star or have a companion or interacting galaxy. We list these galaxies here for completeness, but we do not include them in our candidate list because their photometry is likely to be contaminated by the near neighbor and the luminosities may be overestimated. Among the 14 galaxies, 4 have nearby stars: NGC 2974,<sup>4</sup> NGC 6619, IC 947, UGC 11950; the other 10 have interacting or close companion galaxies: NGC

<sup>4</sup> We note that NGC 2974 was included in ATLAS<sup>3D</sup> but was assigned  $M_K = -23.62$  mag, much fainter than our survey magnitude cut and the 2MASS XSC value  $K = 6.24$  mag and a corresponding  $M_K = -26.16$  mag. The 2MASS isophotal radius is  $71''$  for this galaxy, enclosing the  $V = 9.2$  mag bright star BD-03 2751 that is  $43''$  away. The 2MASS magnitude for NGC 2974 is therefore highly contaminated.

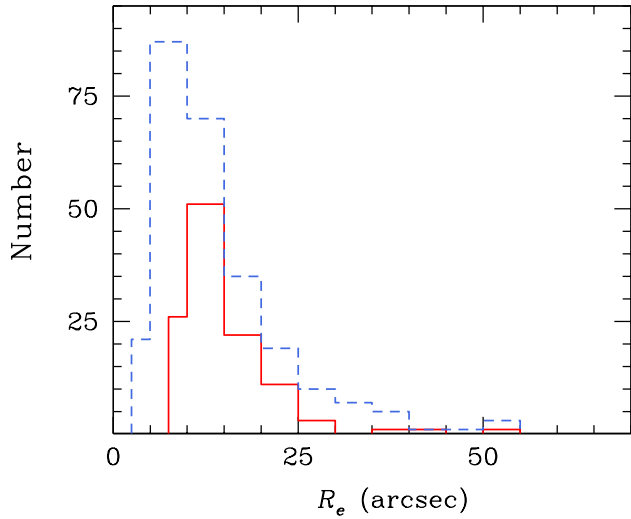


FIG. 3.— Distribution of 2MASS angular sizes for the MASSIVE (red solid) and ATLAS<sup>3D</sup> (blue dashed) galaxies. The Mitchell IFS has a FOV of  $107'' \times 107''$  and probes up to  $\sim 2R_e$  for most MASSIVE galaxies. The FOV of Sauron/ATLAS<sup>3D</sup> is  $33'' \times 41''$ .

71, NGC 750, NGC 1128, NGC 4841A, NGC 5222, NGC 7318, PGC 27509, PGC 93135, UGC 2759, UGC 12591.

One exception is the close galaxy pair NGC 545/547. NGC 547 is in 2MASS and passes our selection cut. NGC 545 is not in 2MASS, but it is listed as the BCG of Abell 194 with  $M_V = -22.98$  mag (Lauer et al. 2007b). We include both galaxies in our sample.

We exclude NGC 1275, the central galaxy in the Perseus Cluster, since it is a complex post-merger system (e.g., Canning et al. 2014, and references therein).

### 3. GALAXY PROPERTIES

#### 3.1. Stellar Mass

A major goal of this survey is to obtain measurements of the stellar mass-to-light ratio of massive early-type galaxies from both dynamical modeling and stellar population synthesis modeling of the IFS kinematic data. In the interim, we estimate the stellar mass of the survey galaxies using a conversion between  $K$ -band luminosity and stellar mass for early-type galaxies in the ATLAS<sup>3D</sup> sample (Cappellari 2013):

$$\log_{10}(M^*) = 10.58 - 0.44(M_K + 23). \quad (2)$$

The relation is fitted between total extinction-corrected 2MASS  $K$ -band magnitudes and dynamical stellar masses from Jeans Anisotropic MGE (JAM), where MGE is the Multi-Gaussian Expansion method (Emmellem et al. 1994). This scaling naturally incorporates any potential IMF changes as a function of mass. Upon the completion of the MASSIVE survey, we will be able to test the validity of this conversion for the mass range  $M^* \gtrsim 10^{11.5} M_\odot$ , which is currently uncalibrated at this high mass.

#### 3.2. Galaxy Size

The 2MASS XSC catalog lists a variety of measurements for galaxy sizes. For ease of comparison, we adopt

a similar definition of the effective radius  $R_e$  as Cappellari et al. (2011). Their  $R_e$  is based on the half-light radius from XSC (parameters `j_r_eff`, `h_r_eff`, and `k_r_eff`). This radius is derived from the 2MASS surface brightness profile in each band as the value of the semi-major axis of the ellipse that encloses half of the total light. We assign each galaxy a 2MASS  $R_e$  using the median value in the three bands:

$$R_e = \text{median}(j\_r\_eff, h\_r\_eff, k\_r\_eff) \sqrt{\text{sup\_ba}}, \quad (3)$$

where the parameter `sup_ba` is the minor-to-major axis ratio measured from the 2MASS 3-band co-added image at the  $3\sigma$  isophote.<sup>5</sup> This factor is included here to convert the semi-major axis into the radius of the circle with the same area. Cappellari et al. (2011) found the 2MASS  $R_e$  for ATLAS<sup>3D</sup> galaxies to correlate well with the optical  $R_e$  from the RC3 catalog (de Vaucouleurs et al. 1991) with an rms scatter of 0.12 dex, but the 2MASS radii were smaller by an overall factor of  $\approx 1.7$ , presumably because 2MASS is shallow (see also Lauer et al. 2007b).

Here we compare the 2MASS  $R_e$  with the optical sizes from the NASA-Sloan Atlas (NSA), which in turn is based on the SDSS DR8 spectroscopic catalog (York et al. 2000; Aihara et al. 2011). This version of the SDSS photometric catalog has a revised sky subtraction designed specifically to mitigate known galaxy size measurement problems for large galaxies (Desroches et al. 2007; Blanton et al. 2011). The NSA provides a unified analysis of local galaxies within  $\sim 200$  Mpc. A total of 77 MASSIVE galaxies are in the NSA. For the optical  $R_e$ , we use the 50% light radius from a 2-dimensional Sérsic fit along the major axis (NSA parameter `SERSIC_TH50`). The Sérsic indices from the NSA fits range from  $n = 2$  to the maximum allowed  $n = 6$ .

The values of 2MASS and available NSA radii are listed in Table 3. Figure 2 compares the physical  $R_e$  from 2MASS and NSA for galaxies in the MASSIVE and ATLAS<sup>3D</sup> surveys. The best-fit relation (black line) is

$$\log_{10} R_e^{2\text{MASS}} = 0.80 \log_{10} R_e^{\text{NSA}} - 0.076, \quad (4)$$

where the radii are in kpc. At  $\sim 1$  kpc, the NSA  $R_e$  is a factor of  $\sim 1.2$  larger than the 2MASS  $R_e$ . At  $\sim 10$  kpc, the offset increases to a factor of  $\sim 1.8$ . This difference underscores the need for deeper photometry, particularly in the  $K$ -band and for massive galaxies.

Figure 3 shows the distributions of the 2MASS angular  $R_e$  for galaxies in the two surveys. Most MASSIVE galaxies are in the range of  $\sim 10''$  to  $50''$ , comparable to those of ATLAS<sup>3D</sup> galaxies. Due to the larger distances, however, the physical sizes of MASSIVE galaxies are  $\sim 2$  to 5 times larger. This is consistent with the large stellar masses of these galaxies. The  $107'' \times 107''$  FOV of our IFS covers up to  $\sim 2R_e$  of most galaxies in the MASSIVE survey, in comparison to the  $33'' \times 41''$  FOV of ATLAS<sup>3D</sup>.

#### 3.3. Stellar Velocity Dispersions

A total of 98 MASSIVE galaxies have stellar velocity dispersion measurements in the HyperLeda database

<sup>5</sup> We use `sup_ba` instead of the  $K$ -band axis ratio `k_ba` adopted by Cappellari et al. (2011) because `sup_ba` is measured from the higher S/N combined images and is listed to 3 rather than 1 decimal precision in 2MASS XSC.

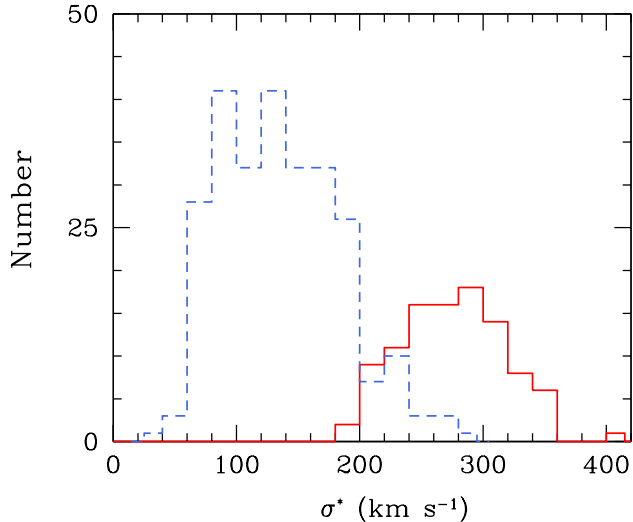


FIG. 4.— Distribution of stellar velocity dispersion for the MASSIVE (red solid) and ATLAS<sup>3D</sup> (blue dashed) galaxies.

(Paturel et al. 2003). Among those not in HyperLeda, five have  $\sigma$  measurements in the SDSS (Bolton et al. 2012). These 103 values are plotted in Figure 4 and listed in Table 3; all other available values of SDSS  $\sigma$  are also listed. The literature  $\sigma$  values are measured over a range of radial apertures, so HyperLeda has homogenized the measurements in a way designed to correct (on average) for aperture effects as well as other differences in technique among different studies (Prugniel & Simien 1996; see also Ho 2007). The HyperLeda measurements are compiled as follows: (i) choose a subsample of galaxies with three or more  $\sigma$  measurements in the literature; (ii) pick those that agree within  $30 \text{ km s}^{-1}$ ; and (iii) for each source, derive offsets to match a gold sample of  $\sigma$ . The final reported dispersion is a weighted mean of scaled values. The corrected velocity dispersions from HyperLeda correspond to an aperture of 0.6 kpc.

The range of  $\sigma$  (Figure 4) for our survey galaxies is large, starting at  $\sim 200 \text{ km s}^{-1}$  up to  $400 \text{ km s}^{-1}$  for NGC 4889. Two galaxies have anomalous  $\sigma$  in HyperLeda: NGC 4059 with  $121 \text{ km s}^{-1}$  and NGC 4055 with  $500 \text{ km s}^{-1}$ . We replace them with  $206 \text{ km s}^{-1}$  and  $270 \text{ km s}^{-1}$ , respectively, from the NSA. Ultimately, our survey will produce spatially-resolved 2-dimensional maps of velocities and will update the  $\sigma$  measurements.

### 3.4. Shape

The shapes, kinematics, and masses of early-type galaxies are closely correlated. Lower-mass elliptical galaxies tend to be fast rotators and have higher ellipticities, whereas giant ellipticals rotate slowly and are round and mildly triaxial (e.g., Binney 1978; Davies et al. 1983; Kormendy & Bender 1996; Tremblay & Merritt 1996). It is therefore interesting to examine the distributions in galaxy shapes for the MASSIVE and ATLAS<sup>3D</sup> samples.

Figure 5 compares the ellipticities,  $\epsilon = 1 - \text{sup\_ba}$ , for galaxies in the two surveys, where  $\text{sup\_ba}$  is the 2MASS XSC parameter for the minor-to-major axis ratio fit to their “super-coadd” isophote. Only five MASSIVE galaxies have high ellipticities with  $\epsilon \gtrsim 0.5$ , in contrast

to about a quarter of the ATLAS<sup>3D</sup> sample. These five galaxies are all in the fainter half ( $M_K \gtrsim -25.7 \text{ mag}$ ) of our sample. Our survey data will provide direct measurements of the spatial profile of the rotation and  $\epsilon$  of each galaxy and will allow us to quantify the distributions of galaxy rotations and shapes at the highest masses.

### 3.5. Color

Galaxies in the MASSIVE survey are selected based on properties such as luminosity and morphology but not color. We quantify their color distribution using the photometry for the 77 MASSIVE galaxies that are in the NSA. We find that the  $u - r$  distribution is well-described as a Gaussian with a mean color of  $u - r = 2.7 \pm 0.06 \text{ mag}$ . This level of scatter is similar to those quoted in earlier work (e.g., Bower et al. 1992; Bernardi et al. 2003b; Blanton et al. 2005; Eisenhardt et al. 2007). The small scatter in the color-magnitude relation is most likely tied to a uniformly old age and a narrow range in stellar metallicity for these galaxies. The wide range of environments of our galaxies (see Sec 4) will enable us to identify any potential color differences among the most massive galaxies as a function of local environments.

### 3.6. Supermassive Black Holes

Seven galaxies in our sample have published black hole masses in the literature: the three Virgo galaxies NGC 4486 (Gebhardt et al. 2011; Walsh et al. 2013), NGC 4472 (Rusli et al. 2013b), and NGC 4649 (Shen & Gebhardt 2010); NGC 3842 and NGC 4889 (McConnell et al. 2011a, 2012); NGC 7052 (van der Marel & van den Bosch 1998), and NGC 7619 (Rusli et al. 2013b). These galaxies are located at the high end of the  $M_{\text{BH}} - M^*$  relation (McConnell & Ma 2013), but due to the large scatter in  $\sigma$  vs  $M^*$  (Figure 13), the high end of the  $M_{\text{BH}} - \sigma$  relation is populated by a mixture of these massive galaxies and several others not massive enough to be in our survey. Recent efforts at measuring large  $M_{\text{BH}}$  have all targeted high- $\sigma$  galaxies (e.g., McConnell et al. 2011a, 2012; van den Bosch et al. 2012; Rusli et al. 2013b). Our survey will provide a complementary sample of  $M_{\text{BH}}$  in galaxies selected based on high stellar mass.

## 4. GALAXY ENVIRONMENTS

In this section we investigate the larger-scale environments of galaxies in the MASSIVE survey. Massive early-type galaxies are commonly assumed to be located at or near the centers of galaxy groups or clusters. Our survey targets the most massive galaxies within a  $\sim 100 \text{ Mpc}$  volume. Where do these  $M^* \gtrsim 10^{11.5} M_{\odot}$  galaxies reside? Below we quantify their environments using three group catalogs constructed from galaxy redshift surveys of the local volume.

### 4.1. 2MRS Group Catalog

Crook et al. (2007, 2008) presents a redshift-limited catalog of groups for the galaxies with  $K < 11.25 \text{ mag}$  in 2MASS XSC. The FOF algorithm with two sets of linking parameters is used to create two group catalogs of differing density contrasts. The high-density-contrast (HDC) catalog lists galaxy membership in groups that have a density contrast of 80 or more, corresponding to linking parameters of  $350 \text{ km s}^{-1}$  along the line of sight and

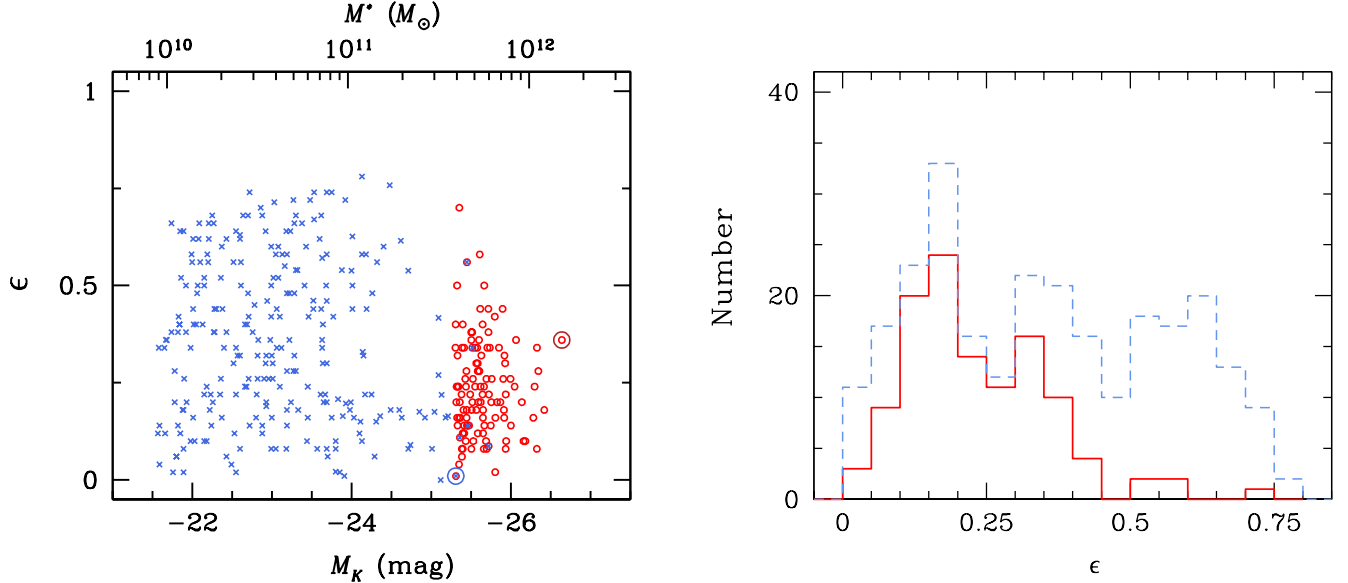


FIG. 5.— Ellipticity versus  $K$ -band luminosity (left panel) and ellipticity distribution (right panel) for galaxies in the MASSIVE survey (red circles) and ATLAS<sup>3D</sup> survey (blue crosses). The ellipticity is  $\epsilon = 1 - \text{sup\_ba}$ , where  $\text{sup\_ba}$  is the 2MASS XSC parameter for the minor-to-major axis ratio fit to their “ $3\text{-}\sigma$  super-coadd isophote.” There is a dearth of high- $\epsilon$  galaxies in the MASSIVE sample. The big circles in the left panel indicate NGC 4889 (red) and M87 (blue).

0.89 Mpc in the transverse directions. The low-density-contrast (LDC) catalog is constructed with larger linking lengths of  $399 \text{ km s}^{-1}$  and 1.63 Mpc, corresponding to a density contrast of 12 or more.

The exact membership of groups in any group/cluster catalog depends on the algorithm and linking parameters used to construct the catalog. All galaxies assigned to groups in the HDC catalog are also assigned to groups in the LDC catalog, but the converse is not true. The larger linking lengths used in LDC tend to merge smaller groups and generate more extended structures, whereas large structures tend to be fragmented into individual groups in HDC. Three galaxies in Virgo are bright enough to be in our survey; they are assigned to a single group of 205 members in HDC, and a single group of 300 members in LDC. Similarly, the four brightest galaxies in the Coma cluster are in our survey. They are all properly assigned to a single group in both the HDC and LDC catalogs, containing 49 and 84 members, respectively.

Two measurements of the mass of each group are provided in Crook et al. (2007), one based on the virial estimator and the other based on the projected mass estimator. The virial mass estimator is computed from the line-of-sight velocity dispersion and mean harmonic projected separation of group members. The latter quantity is sensitive to close pairs and can be noisy, in particular for groups not uniformly sampled spatially. The projected mass estimator (Heisler et al. 1985) is designed to give equal weights to group members at all distances. This mass estimator depends on the mean eccentricity of the orbits and is parameterized by an overall coefficient  $f_{\text{pm}}$  that typically is not measured and must therefore be assumed. The parameter  $f_{\text{pm}}$  ranges from  $32/\pi$  for isotropic orbits to  $64/\pi$  for radial orbits, independent of the mass distribution. The Crook et al. (2007) catalog

TABLE 2  
ENVIRONMENT OF MASSIVE GALAXIES

Environment	HDC	LDC	2M++
Groupless	26	12	23
In groups	90	104	93
Brightest group galaxy	65	70	70

Notes. Number of MASSIVE galaxies that are (1) group-less, i.e., “isolated” and have no group members; (2) in groups of three or more members; and (3) the brightest galaxy in its group. Three galaxy group catalogs (all based on 2MASS) are shown: the high-density-contrast (HDC) and low-density-contrast (LDC) catalogs of Crook et al. (2007) and the 2M++ catalog (Lavaux & Hudson 2011).

assumes  $f_{\text{pm}} = 32/\pi$ , which yields the smallest mass.

Table 2 lists the statistics of the environment of our candidate galaxies classified by the HDC and LDC group catalogs. As expected, more galaxies are identified as being in groups in the LDC catalog. Figure 6 plots the distribution of the virial halo mass of the HDC groups in which the MASSIVE galaxies reside. The black histogram shows the halo distribution of all 90 galaxies in groups, and the red histogram plots the subset of 65 brightest group galaxies (BGGs). The agreement of the two histograms at  $M_{\text{halo}} \lesssim 10^{13.75} M_\odot$  indicates that the 39 MASSIVE galaxies in these lower-mass groups are all BGGs. By contrast, only 26 of the 51 galaxies in the higher-mass groups are BGGs.

#### 4.2. 2M++ Group Catalog

As a comparison study, we examine the environmental properties of the MASSIVE galaxies in the 2M++ galaxy redshift catalog of Lavaux & Hudson (2011). This more

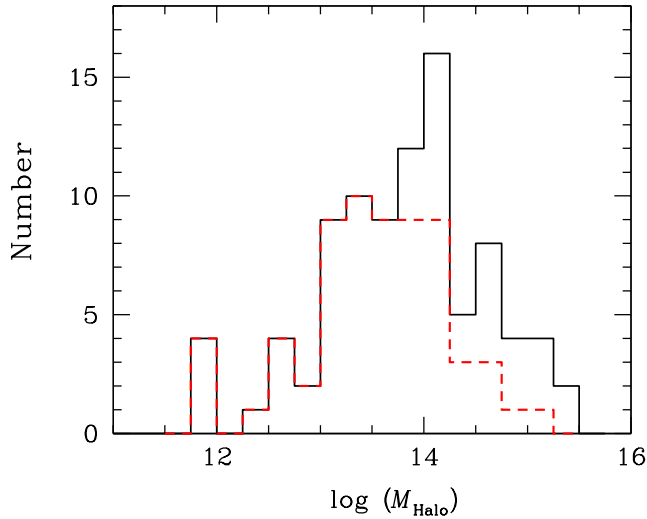


FIG. 6.— Distribution of dark matter halo masses for the 90 MASSIVE galaxies that reside in groups in the HDC catalog (black histogram). The halo mass is obtained from the virial mass estimator (Sec 4.1). Among the 90, 65 are the brightest group galaxies (BGG) in their respective groups (red histogram). The two histograms show that the 39 MASSIVE galaxies in the lower-mass groups are always the BGGs, whereas for those in groups with  $M_{\text{halo}} \gtrsim 10^{13.75} M_{\odot}$ , about 50% are not BGGs.

recent compilation of 69,160 galaxy redshifts is based on the 2MASS photometric catalog for target selection and uses primarily the redshifts from SDSS-DR7, 6dGFRS, and 2MRS. The catalog covers nearly the full sky and reaches depths of  $K = 12.5$ , in comparison to  $K = 11.75$  mag for 44,599 galaxies in 2MRS. Groups in this catalog are identified by the FOF algorithm with linking parameters of 0.64 Mpc and  $1000 \text{ km s}^{-1}$ . The corresponding overdensity threshold of 80 is the same as the HDC catalog of Crook. The group list contains 4002 groups with three or more members up to redshift distance of  $20,000 \text{ km s}^{-1}$ . The members of the nearest two clusters Virgo and Fornax are not properly identified by the FOF algorithm and are assigned manually.

A total of 93 MASSIVE galaxies are identified to reside in groups by the 2M++ catalog, similar to 90 in HDC (see Table 2). Figure 7 shows that the numbers of group members are reasonably consistent between the two catalogs. For the handful of galaxies that are assigned to a group in one catalog but not in the other, most of them reside in small groups of low velocity dispersion and low membership, a regime that is more sensitive to the different linking parameters and parent samples used in the two catalogs.

#### 4.3. Groupless Galaxies

Not all MASSIVE galaxies are associated with groups (of three or more members) in the Crook or 2M++ catalogs: 26 galaxies are not in groups according HDC, and 23 galaxies are not in 2M++ groups. Among these, 17 galaxies are groupless in both catalogs. These galaxies are relatively isolated and presumably live in low-density environments. Any satellite galaxy, if present, is likely to be faint.

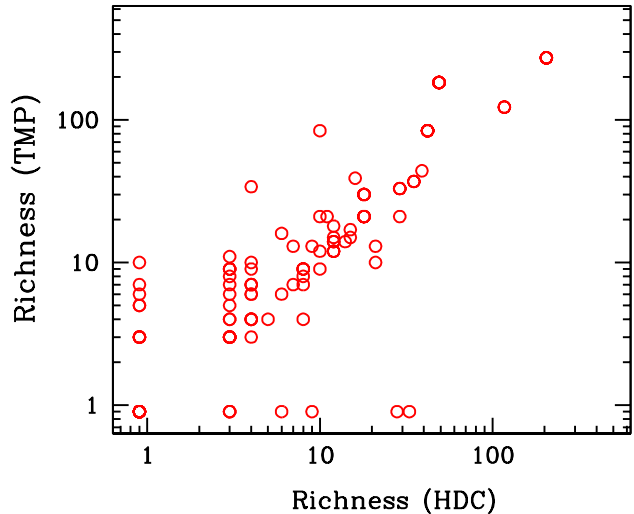


FIG. 7.— Comparison of group membership in the 2MRS HDC catalog and 2M++ catalog for MASSIVE galaxies. The points with richness below 1 along each axis represent galaxies that are identified to reside in groups by only one catalog. These are mostly lower-mass groups with a handful of members.

A handful of these 17 groupless galaxies had been targeted for X-ray observations. Three have archival Chandra and/or XMM-Newton observations: NGC 57, NGC 4555, and NGC 7052. The X-ray luminosity of the thermal component in the 0.52 keV band for the three galaxies are:  $10^{41.19 \pm 0.02} \text{ erg s}^{-1}$  (NGC 57),  $10^{41.27 \pm 0.04} \text{ erg s}^{-1}$  (NGC 4555), and  $10^{41.17 \pm 0.02 - 0.03} \text{ erg s}^{-1}$  (NGC 7052) (Mulchaey & Jeltama 2010). The X-ray halos of NGC 57 and NGC 4555 both have  $kT \sim 0.9 \text{ keV}$  and extend to 50 to 60 kpc (O’Sullivan & Ponman 2004; O’Sullivan et al. 2007). NGC 7052 has an X-ray halo of  $kT \sim 0.48 \text{ keV}$  (Memola et al. 2009) and a central AGN with  $L_x \sim 3 \times 10^{40} \text{ erg s}^{-1}$  (Donato et al. 2004).

These groupless galaxies and other galaxies in low-richness groups in our survey form an interesting subsample of targets for further studies. For instance, we are investigating whether the groupless galaxies have faint optical companions and satisfy the criterion of being fossil groups (Ponman et al. 1994; Jones et al. 2003). Overall, our survey galaxies span only a factor of  $\sim 3$  in stellar mass (Figure 1) but a much wider range in halo mass (Figure 6) and group membership (Figure 7), providing an excellent sample for studying environmental effects on galaxy formation (Mulchaey & Jeltama 2010).

## 5. OBSERVATIONS

### 5.1. Large-format IFS

Our large-scale IFS observations are performed with the Mitchell Spectrograph (Hill et al. 2008) on the 2.7 m Harlan J. Smith Telescope at McDonald Observatory. The Mitchell Spectrograph is an optical integral-field spectrograph with a large field of view ( $107'' \times 107''$ ) and 4.1'' diameter fibers. The 246 fibers are evenly-spaced and assembled in an array similar to Densepak on the WIYN telescope (Barden et al. 1998) with a one-third filling factor.



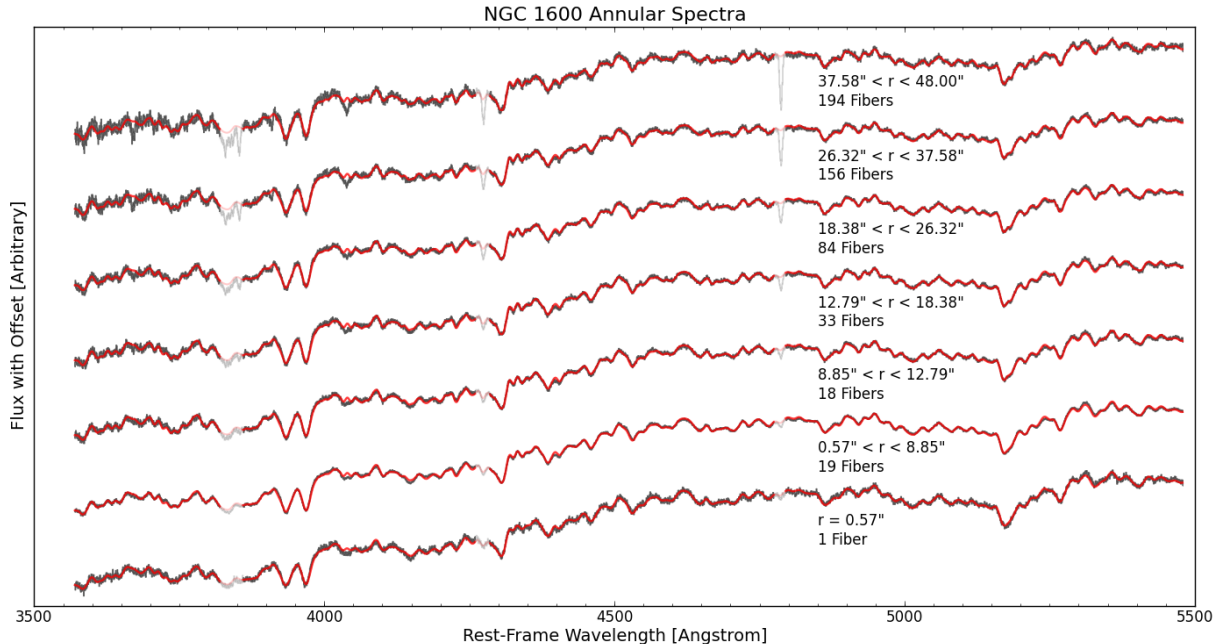


FIG. 8.— Mitchell spectra for NGC 1600 in 7 radial bins. The bin size and number of fibers in each bin are labeled. The best-fit spectra from pPXF are overlaid in red.

We use the low-resolution blue setting ( $R \approx 850$ ) of the Mitchell Spectrograph. The wavelength coverage spans 3650 to 5850Å, including the Ca H+K region, the G-band region,  $H\beta$ , the  $Mgb$  region, and several Fe absorption features. The spectral resolution varies spatially and with wavelength but has an average of  $5\text{\AA}$  FWHM, corresponding to a dispersion of  $\sim 1.1\text{\AA pixel}^{-1}$  and  $\sigma \sim 100\text{ km s}^{-1}$  in the red part of the spectrum to  $\sim 150\text{ km s}^{-1}$  in the blue part.

We observe each galaxy with three dither positions of equal exposure time to obtain a contiguous coverage of the field of view. For each dither position, we interleave a ten-minute exposure on sky with two twenty-minute on-target science frames. Each galaxy is therefore observed for a total of  $\approx 2$  hours on source. With this observing strategy, we typically reach S/N above 50 in the central fiber alone. For the outer fibers, we co-add the fibers and create spatial bins with a minimum of  $S/N=20$  per bin. Our binning procedure provides a good combination of spatial resolution and S/N, resulting in  $\sim 30$  to 60 spatial bins per galaxy and a median S/N from 25 to more than 30 for each of the ten galaxies we have analyzed thus far. Even in the outermost radial bin covered by the IFU, our data have sufficient S/N to provide multiple angular bins (see example in Figs. 9 and 10). Comparable S/N requirements are used for dynamical orbit modeling of luminous and dark matter in Coma galaxies (Thomas et al. 2007) and for  $M_{\text{BH}}$  measurements using combined wide-field and AO IFU data (e.g. Rusli et al. 2013b; McConnell et al. 2012). With these data, we expect to constrain stellar population gradients larger than roughly a tenth of a dex per decade in radius (e.g.,

Greene et al. 2013). In a handful of galaxies, we have integrated substantially longer (i.e., 6-8 hours) on an off-nucleus pointing (e.g., Murphy et al. 2011). With these cases we are able to roughly double our radial coverage at comparable S/N.

The data reduction is performed using the Vaccine package (Adams et al. 2011; Murphy et al. 2011). Flux calibration and final reduction are done with the software developed for the VENGGA project (Blanc et al. 2009, 2013). The flux calibration is quite robust, with  $< 10\%$  disagreement in continuum shape between the central Mitchell fiber and SDSS spectra when available (Greene et al. 2012, 2013). Figure 8 shows the spectra for a range of radial bins for NGC 1600 from our Mitchell IFS data taken in October 2013. The resulting stellar kinematics and stellar populations for NGC 1600 are presented in Sec. 6 below.

In 2010 we conducted a precursor study to MASSIVE with the Mitchell spectrograph (Greene et al. 2012). Galaxies were selected to have red colors ( $u-r > 2.2$ ) and velocity dispersions  $> 150\text{ km s}^{-1}$  (as measured by the SDSS) within the redshift range  $0.01 < z < 0.02$ . The galaxies span a mass range of  $M^* \approx 10^{10.4-11.5} M_{\odot}$ , less massive than MASSIVE galaxies but still generally more massive than the ATLAS<sup>3D</sup> galaxies. Fifty galaxies have been observed to date, and we analyzed their stellar population properties in Greene et al. (2013) and their kinematic properties in Raskutti et al. (2014). Because they were observed in an identical manner to the MASSIVE galaxies, we will use them as a complementary sample for comparison studies.

### 5.2. AO-assisted IFS

For a subset of MASSIVE galaxies suitable for AO-assisted observations, we are acquiring high-resolution data to perform new measurements of black hole masses  $M_{\text{BH}}$  using stellar dynamics. We use NIFS and the ALTAIR adaptive optics system with both natural guide star (NGS) and laser guide star (LGS) on the 8 m Gemini Observatory North telescope, and OSIRIS (Larkin et al. 2006) and LGS-AO system on the 10 m W. M. Keck I telescope.

The literature contains  $M_{\text{BH}}$  measurements for seven galaxies in our MASSIVE sample (see Sec 3.6). We are preparing  $M_{\text{BH}}$  measurements for six additional MASSIVE galaxies based on our existing AO data; seeing-limited IFS data at  $\sim 0.4''$  resolution may yield up to four more. Our ongoing campaign with AO instruments will extend the sample of  $M_{\text{BH}}$  in MASSIVE galaxies still further.

Because MASSIVE galaxies are selected for extreme stellar masses, and because they mostly lie within a factor of two in distance (54-108 Mpc), much of the variation in the angular sizes of influence of the central black holes results from the cosmic scatter in  $M_{\text{BH}}$ . In this case the primary limiting factor for AO selection is central surface brightness: fainter than  $\mu_K = 13.5 \text{ mag arcsec}^{-2}$ , high-resolution observations are prohibitively expensive. Within the acceptable range of surface brightnesses, we typically require four to eight hours of AO observations per target, including science and sky frames, calibration stars, and overheads.

### 5.3. Deep $K$ -band Imaging

Most of our science goals require a deep luminosity profile for each galaxy. Since 2MASS is shallow, we are obtaining deeper  $K$ -band imaging for the MASSIVE sample using a combination of WFCAM on UKIRT and WIRCAM on CFHT. We choose  $K$ -band because it (i) traces the old populations that compose most of the stellar mass in early-type galaxies; (ii) minimizes dust extinction; (iii) allows for uniform calibration using 2MASS; and (iv) facilitates comparison of black hole masses across galaxy populations via the  $M_{\text{BH}} - L_K$  relation.

In order to trace the extended halos of luminous early-type galaxies and measure accurate total magnitudes, it is desirable to reach a surface brightness limit  $\sim 3 \text{ mag arcsec}^{-2}$  fainter than 2MASS (cf. Appendix B of Lauer et al. 2007b). The 2MASS  $3\sigma$   $K$  surface brightness limit is  $\mu_K = 18.6 \text{ mag arcsec}^{-2}$  (Jarrett et al. 2000), which corresponds roughly to the often quoted  $1\sigma$  value of  $\mu_K \sim 20 \text{ mag arcsec}^{-2}$ . Thus, in terms of AB mag, we are aiming to achieve a  $3\sigma$  surface brightness limit of  $\sim 23.6 \text{ mag arcsec}^{-2}$  (3 mag in depth plus 2 mag AB conversion).

## 6. EXAMPLES OF SURVEY SCIENCE AND EARLY RESULTS

The MASSIVE survey is designed to study the most massive galaxies in the universe today, a parameter space that has not been systematically explored with IFS to date. With the nearly  $2'$  field of view of the Mitchell spectrograph, we cover about twice the effective radius of most galaxies in the survey. The additional AO data

for a subset of the galaxies will probe sub-arcsec scales down to the gravitational sphere of influence of the central supermassive black hole ( $\sim 100 \text{ pc}$ ). In the following sections we discuss key science results that can be expected from the survey and present some early results. This list is by no means exhaustive.

### 6.1. Stellar Mass-to-Light Ratio and IMF

Our kinematic measurements at large radius, combined with Schwarzschild orbit modeling, allow us to measure the dark matter halo mass and the dynamically inferred stellar mass-to-light ratio  $(M^*/L)_{\text{dyn}}$ . At the same time, stellar population synthesis modeling of our Mitchell spectra in the blue combined with our  $K$ -band imaging and space-based photometry in the mid-infrared provide an independent measurement of the stellar mass, yielding  $(M^*/L)_{\text{pop}}$ .

The observed increase in the ratio of  $(M^*/L)_{\text{dyn}}/(M^*/L)_{\text{pop}}$  in galaxies with increasing  $\sigma$  has been interpreted as a change in the IMF (e.g., Treu et al. 2010; Auger et al. 2010; Cappellari et al. 2012; Sonnenfeld et al. 2012; Tortora et al. 2013; Dutton et al. 2013; Barnabè et al. 2011, 2013), but it could also indicate a degeneracy with the dark matter distribution (e.g. Thomas et al. 2011; Wegner et al. 2012). A number of independent approaches, including direct measurements of gravity-sensitive stellar features and gravitational lensing, have pointed towards an IMF that becomes more top-heavy in galaxies with higher stellar velocity dispersions (e.g., Conroy & van Dokkum 2012; Spiniello et al. 2014; Oguri et al. 2014). Some recent results, however, are not consistent with an increasingly top-heavy IMF in all systems (e.g., Smith & Lucey 2013; Rusli et al. 2013b; Smith 2014). The sample size and dynamic range in mass of the MASSIVE survey will improve the constraints on any possible mass dependence of the IMF.

As a demonstration of early results from our survey, we show in Figure 9 the 2-dimensional stellar kinematic maps for NGC 1600. We use the penalized pixel-fitting (pPXF) method (Cappellari & Emsellem 2004) to extract the stellar line-of-sight velocity distribution (LOSVD) function  $f(v)$  from the absorption line features in our spectra. As input templates, we use the MILES library of 985 stellar spectra, covering the wavelength range of 3525-7500Å at 2.5Å (FWHM) spectral resolution (Sánchez-Blázquez et al. 2006). The pPXF routine convolves the MILES stellar templates with  $f(v)$  modeled as a Gauss-Hermite series (up to order 6):

$$f(v) \propto \frac{1}{\sqrt{2\pi\sigma^2}} e^{-\frac{(v-V)^2}{\sigma^2}} \left[ 1 + \sum_{m=3}^n h_m H_m \left( \frac{v-V}{\sigma} \right) \right], \quad (5)$$

where  $H_m(x)$  is the  $m$ th Hermite polynomial and given by

$$H_m(x) = \frac{1}{\sqrt{m!}} e^{x^2} \left( -\frac{1}{\sqrt{2}} \frac{\partial}{\partial x} \right)^m e^{-x^2}. \quad (6)$$

Figure 9 shows the 2-dimensional maps of the best-fit Gauss-Hermite velocity moments  $V, \sigma, h_3$ , and  $h_4$  from our Mitchell IFS observations of NGC 1600. The galaxy rotates slowly with  $V \lesssim 20 \text{ km s}^{-1}$  about its photometric minor axis. The velocity dispersion peaks at  $360 \text{ km s}^{-1}$

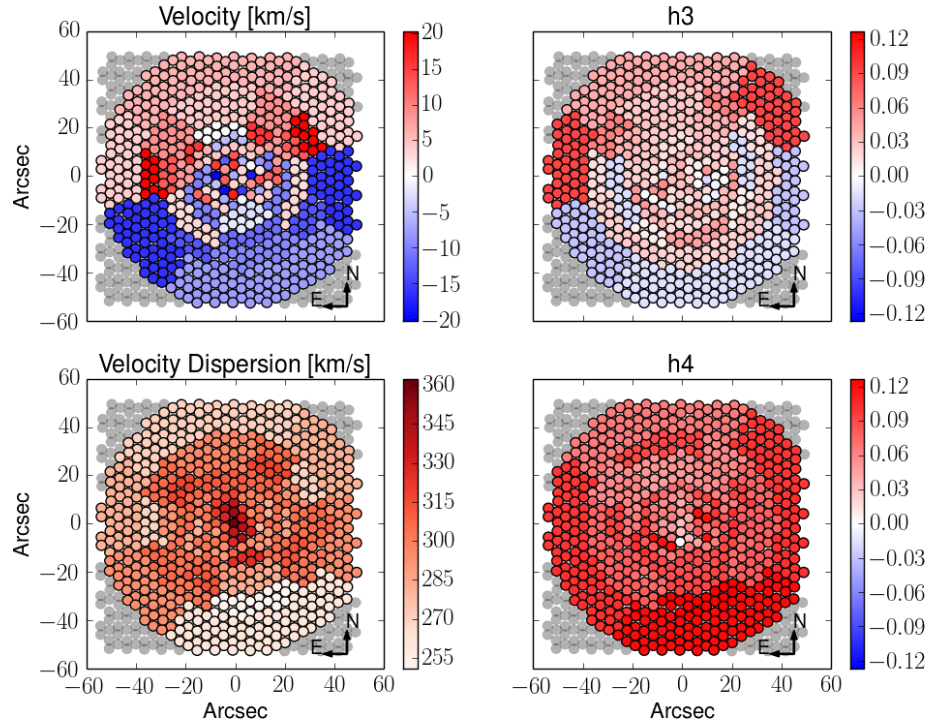


FIG. 9.— Kinematic maps of the line-of-sight velocity moments for NGC 1600. The four panels show the four Gauss-Hermite moments,  $V$ ,  $\sigma$ ,  $h_3$ , and  $h_4$ , respectively. The circles in each panel indicate the Mitchell IFS fibers. The fibers are grouped into spatial bins to ensure a minimum S/N of 20; the median S/N of the bins is 30.6 for NGC 1600. Individual fibers near the center have S/N  $\sim$  60. The median errors over the spatial bins for the four moments are  $17 \text{ km s}^{-1}$ ,  $24 \text{ km s}^{-1}$ , 0.051, and 0.057, respectively.

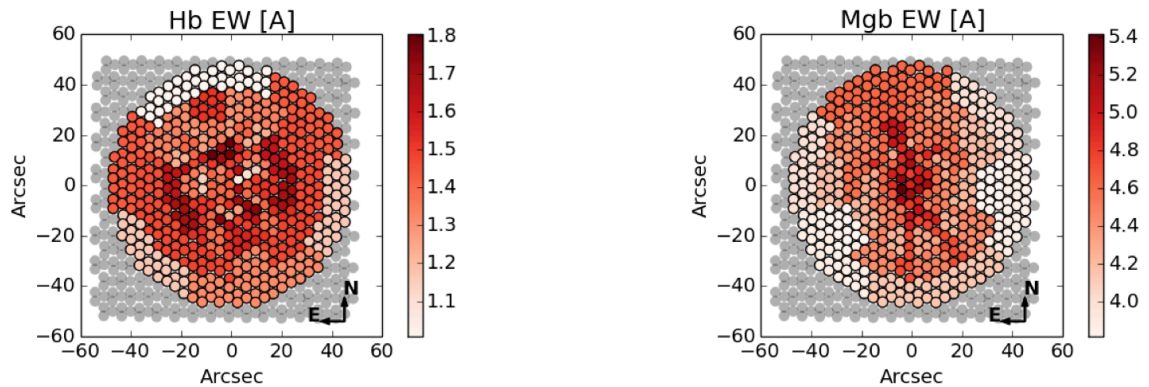


FIG. 10.— Two-dimensional maps of the equivalent widths (in Angstroms) of the  $H\beta$  (left) and  $Mgb$  (right) absorption lines in NGC 1600. Our Mitchell data have sufficient S/N to provide measurements in several angular bins at each radius. The typical errors are  $0.2 \text{ \AA}$  to  $0.3 \text{ \AA}$ .

in the central fiber and declines radially by  $\sim 20\%$  out to  $\sim 50''$ . The flux-weighted  $V/\sigma$  is  $0.03 \pm 0.01$  for NGC 1600. Only two galaxies have such low  $V/\sigma$  in ATLAS<sup>3D</sup> (Emsellem et al. 2011). We will discuss in separate papers the details of this analysis, results for  $(M^*/L)_{\text{dyn}}$ , and tests of systematics including spectral regions used in the fits and robustness of the higher-order Gauss-Hermite moments (J. Thomas et al. 2014, in prep.; R. Janish et al. 2014, in prep.).

### 6.2. Radial Gradients and Assembly History

Massive early-type galaxies have experienced dramatic size evolution, by factors of 2-4, from  $z \approx 2$  to the present (e.g., van Dokkum et al. 2008). One way to understand the physical mechanisms responsible for this growth is to study spatial gradients in the stellar populations and kinematics beyond the half-light radius of present-day ellipticals. Since the dynamical times in the outskirts of these galaxies are long, the stars can potentially remember their origin both in their overall distribution (Naab et al. 2007; Oser et al. 2010; Hilz et al. 2013) and their degree of angular momentum (e.g., Davies et al. 1983; Franx et al. 1991; Krajnović et al. 2011; Wu et al. 2014; Arnold et al. 2014; Naab et al. 2014; Krajnović et al. 2013; Raskutti et al. 2014).

Sensitive spectroscopic observations of stellar populations at large radius are still relatively scarce (e.g., Carollo & Danziger 1994; Mehlert et al. 2003; Kelson et al. 2006; Weijmans et al. 2009; Spolaor et al. 2010; Pu et al. 2010; Pastorello et al. 2014; Martín-Navarro et al. 2014; Greene et al. 2012, 2013). The MASSIVE survey will contribute the largest set of IFS data to date for slowly rotating nearby early-type galaxies in a wide range of large-scale environments. In combination with our deep  $K$ -band imaging, we will also investigate any correlations between rotation as a function of radius and isophotal shape (e.g., Bender et al. 1989; Arnold et al. 2014).

Figure 10 shows the 2-dimensional maps of the equivalent widths (EW) of the  $H\beta$  (left) and  $Mgb$  (right) absorption features for NGC 1600. We measure the standard Lick indices (Faber et al. 1985; Worthey et al. 1994) using the IDL code *lick\_ew* (Graves & Schiavon 2008). In Greene et al. (2012) we demonstrated that because these indices are defined for flux-calibrated spectra, our measurements are on a standard system without any additional offsets. Very low levels of emission-line infill can often contaminate our EW measurements, particularly of  $H\beta$  (e.g., Graves et al. 2007). We perform an iterative fit (Greene et al. 2013) to the  $H\beta + [\text{O III}]$  region, using the stacked spectra from Graves et al. (2009) as templates. Our uncertainties are dominated by sky subtraction, so we scale our fiducial sky model by up to  $\pm 5\%$  and repeat our full procedure to determine the uncertainties. Given our typical S/N ratios of 30 - 100 at  $\sim 2R_e$ , we achieve S/N of 15-80 in the  $H\beta$  and  $Mgb$  line indices at the outer edge of the Mitchell IFU.

Figure 10 shows a characteristic radial decline in  $Mgb$  EW, mostly due to the well-known decline in metallicity with radius in these early-type galaxies. In contrast, the  $H\beta$  EW is relatively flat with radius, with perhaps a subtle trend of falling at the outer parts, reflecting the uniform old age of this galaxy.

### 6.3. Black Hole-Galaxy Correlations

New kinematic data and modeling efforts in the past several years have substantially expanded and revised dynamical measurements of  $M_{\text{BH}}$ . As samples of dynamical black hole masses increase at both the highest masses (e.g., McConnell et al. 2011a,b, 2012; Rusli et al. 2011, 2013b; van den Bosch et al. 2012; Walsh et al. 2013) and in spiral galaxies (e.g., Greene et al. 2010; Kuo et al. 2011; Beifiori et al. 2012; Sun et al. 2013), it becomes increasingly clear that more data are needed to better quantify the intrinsic scatter and mass dependence in the scaling relations between  $M_{\text{BH}}$  and properties of their host galaxies (McConnell & Ma 2013; Kormendy & Ho 2013).

A systematic survey of dynamical black hole masses in the most massive galaxies (without preselection based on current scaling relations) will substantially improve our leverage on the intrinsic scatter in the relations as a function of mass, which may discriminate between different models for galaxy-black hole coevolution (e.g., Peng 2007; Hirschmann et al. 2010; Jahnke & Macciò 2011; Anglés-Alcázar et al. 2013). Knowledge of the intrinsic scatter in  $M_{\text{BH}}$  is crucial for calculating the quiescent black hole mass function, as is understanding whether stellar mass or stellar velocity dispersion is a better predictor of black hole mass (e.g., Lauer et al. 2007b,a). In addition to providing key constraints on current theories of black hole and galaxy growth, these scaling relations are also a critical input in numerous applications that rely on black hole demographics, e.g., the predicted contributions from merging supermassive black hole binaries to the gravitational wave background targeted by the ongoing pulsar timing experiments (van Haasteren et al. 2011; Demorest et al. 2013; Shannon et al. 2013) and LISA.

Cores in central light profiles within a few 100 pc are often seen in massive galaxies. These cores are thought to be a sign of black hole scouring (Begelman et al. 1980), consistent with several scaling relations between core size and other galaxy properties (e.g., Faber et al. 1997; Ferrarese et al. 2006; Lauer et al. 2007b; Kormendy & Bender 2009; Rusli et al. 2013a). As part of our dynamical modeling, we see evidence for an excess of tangential orbits at the galaxy centers, consistent with black hole scouring. We will use our orbit modeling to investigate the connection between the central black hole mass and nuclear galaxy structure.

Figure 11 shows two-dimensional stellar kinematics for the central region of NGC 5557 from our observations with NIFS and LGS-AO on Gemini North. We use stellar templates from Gemini's NIFS/GNIRS template library and fit LOSVD-convolved templates to the  $K$ -band CO bandhead features in each galaxy spectrum. Figure 11 shows the resulting four Gauss-Hermite velocity moments as defined in Equation (5). When applied to stellar orbit, our combined NIFS and Mitchell data yield a black hole mass of  $3.9^{+1.0}_{-1.3} \times 10^9 M_{\odot}$  in NGC 5557 (McConnell et al. 2014, in prep.).

### 6.4. The $R_e - L$ and $\sigma - L$ Relations

The tight scaling relations among size, luminosity, and stellar velocity dispersion of early-type galaxies (e.g., Faber & Jackson 1976; Kormendy 1977; Dressler et al. 1987) have long been used to constrain galaxy assembly

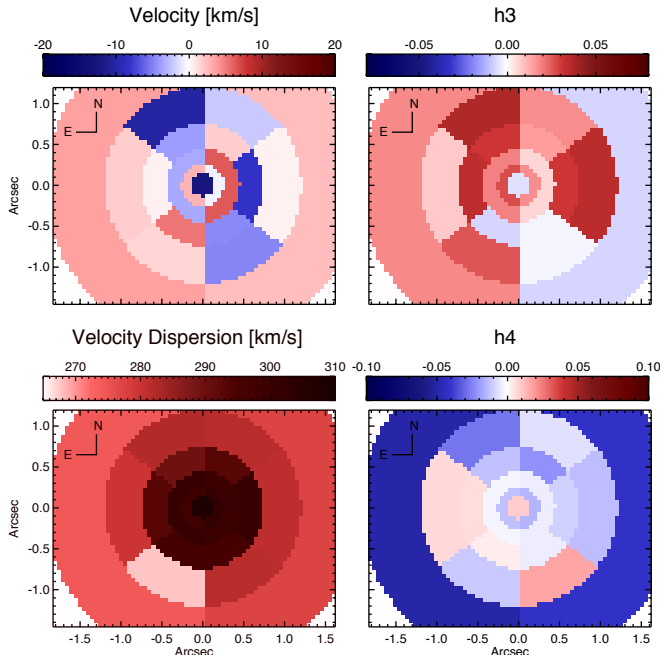


FIG. 11.— Kinematic maps of the line-of-sight velocity moments for the inner  $3'' \times 2''$  region of NGC 5777 from Gemini NIFS. The moments are defined the same way as in Figure 9. The median errors are  $4.6 \text{ km s}^{-1}$  in  $V$ ,  $5.4 \text{ km s}^{-1}$  in  $\sigma$ ,  $0.016$  in  $h_3$ , and  $0.015$  in  $h_4$ .

(e.g., Boylan-Kolchin et al. 2005; Robertson et al. 2006, and references therein). With our spatially resolved stellar kinematics and deep  $K$ -band imaging, we will refine the measurements of the galaxy scaling relations by adding galaxies at the most massive end (e.g., Bernardi et al. 2003a).

Figure 12 plots the 2MASS  $R_e$  and  $M_K$  relation (e.g., Kormendy 1977) for MASSIVE and ATLAS<sup>3D</sup> galaxies. Figure 13 shows the stellar velocity dispersion and  $M_K$  for the 103 MASSIVE galaxies with existing  $\sigma$  measurements. We emphasize that no cuts are made on either  $R_e$  or  $\sigma$  in our sample selection. These plots are only meant to illustrate the demographics of our survey galaxies based on currently available data. We will improve these measurements to address possible biases in 2MASS  $M_K$  (Sec 2.3) and massive galaxy sizes (e.g., Bernardi et al. 2012) and to study the distribution of our galaxies in projections of the fundamental plane (e.g., Lauer et al. 2007b; Kormendy et al. 2009).

### 6.5. X-Ray Gas and Halo Mass

Roughly 30% of the galaxies in the MASSIVE survey have archival Chandra/XMM X-ray observations that are sensitive enough to detect thermal emission from the hot halo gas. If the gas is in thermal equilibrium, then the ratio  $L_X/M^*$  reflects the ratio of dark matter halo to stellar mass. Empirically, large scatter (factor of  $\sim 100$ ) is found between  $L_X$  and  $L_K$  (e.g., Forman et al. 1985; Fabbiano 1989), and there are hints that the

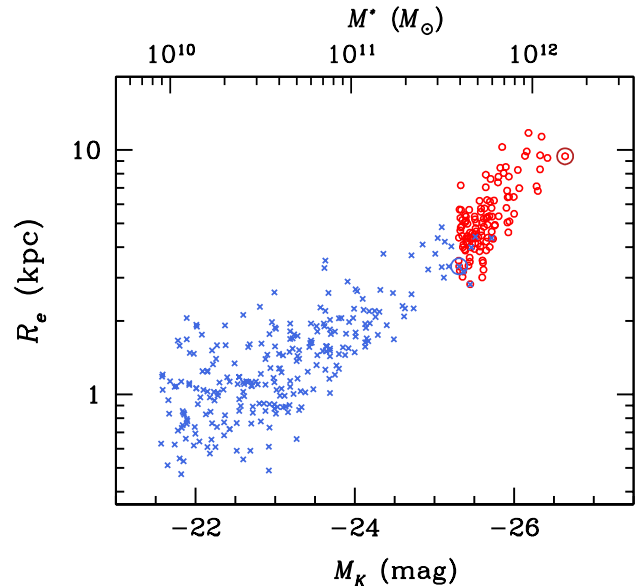


FIG. 12.— 2MASS effective radius versus absolute  $K$ -band magnitude for galaxies in the MASSIVE (red circles) and ATLAS<sup>3D</sup> surveys (blue crosses). The big circles indicate NGC 4889 (red) and M87 (blue).

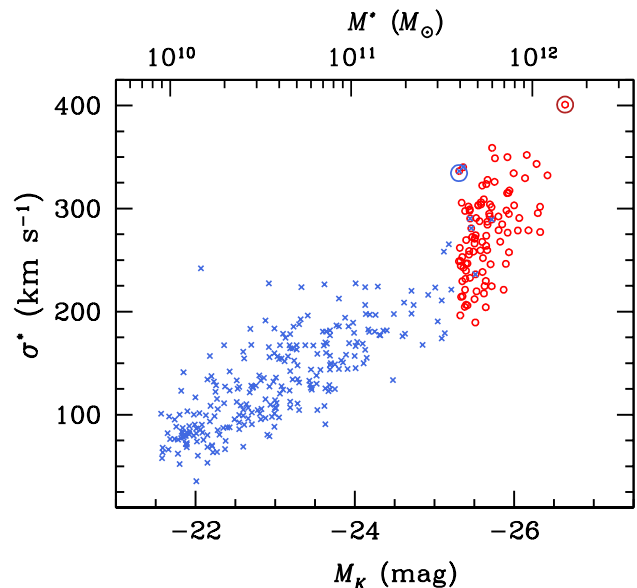


FIG. 13.— Stellar velocity dispersion versus absolute  $K$ -band magnitude for galaxies in the MASSIVE survey (red circles) and ATLAS<sup>3D</sup> survey (blue crosses). A total of 103 MASSIVE galaxies have measured  $\sigma$  in HyperLeda and/or NSA. The big circles indicate NGC 4889 (red) and M87 (blue).

slope and scatter depend on environment (Mulchaey & Jeltama 2010). Likely at play are both intrinsic scatter in the relation between stellar and dark halo mass, and non-equilibrium conditions in the hot gas, e.g., due to AGN feedback (Diehl & Statler 2008; Dunn et al. 2010).

There is a hint of a tighter correlation between  $L_X$  and total dynamical mass (stellar and dark matter halo) than  $L_K$  (Mathews et al. 2006; Kim & Fabbiano 2013), but the sample with independent dynamical halo masses and deep X-ray observations is small, and M87 is still the most massive galaxy included. With MASSIVE, we will revisit the  $L_X/L_K$  and  $L_X/M_{\text{tot}}$  relations for a large and well-defined sample with uniform dynamical halo masses and a range of environments. We may also explore the importance of radio jets in keeping the halo gas from cooling (Allen et al. 2006; McNamara & Nulsen 2007).

## 7. SUMMARY

MASSIVE is a comprehensive IFS survey of a volume-limited and mass-selected sample of the most massive early-type galaxies within  $\sim 108$  Mpc. MASSIVE is the first IFS survey to specifically target galaxies with  $M^* > 10^{11.5} M_{\odot}$ . We exploit the large ( $107'' \times 107''$ ) areal coverage of the Mitchell Spectrograph to obtain stellar population and kinematic information beyond twice the effective radius of our galaxies, while using AO-assisted IFS data on small scales to probe the sphere of influence of the supermassive black hole. The sample galaxies span a narrow range in stellar mass, but a wide range in stellar velocity dispersion, size, halo mass and large-scale environment. Thus, we are poised to determine the rela-

tionships between central black hole mass, stellar mass, and dark halo mass for the most massive galaxies in the universe today.

We thank Joshua Adams, Akos Bogdan, Stephen Chen, Bill Forman, Jim Gunn, and Christine Jones for useful discussions. This survey is supported in part by NSF AST-1411945 and AST-1411642. C.-P.M. is supported in part by grants from the Simons Foundation (No. 224959) and NSF AST-1009663. N.J.M. is supported by the Beatrice Watson Parrent Fellowship. J.D.M. is supported by an NSF Astronomy and Astrophysics Postdoctoral Fellowship (AST-1203057). We thank the Cynthia and George Mitchell Foundation for funding the Mitchell Spectrograph, and Gary J. Hill and Phillip MacQueen on their continued work to make the Mitchell Spectrograph a successful instrument. Dave Doss, Kevin Meyer, Brian Roman, John Kuehne, Coyne Gibson and all of the staff at McDonald Observatory have helped immensely with collection of these data.

This research has made use of the HyperLeda database and the NASA/IPAC Extragalactic Database (NED) which is operated by the Jet Propulsion Laboratory, California Institute of Technology, under contract with the National Aeronautics and Space Administration.

## APPENDIX

TABLE 3  
116 CANDIDATE MASSIVE GALAXIES

Galaxy	R.A. (deg)	Dec. (deg)	$D$ (Mpc)	$K$ (mag)	$A_V$ (mag)	$M_K$ (mag)	$\sigma^{\text{HL}}$ (km/s)	$\sigma^{\text{NSA}}$ (km/s)	$R_e^{2\text{MASS}}$ (arcsec)	$R_e^{\text{NSA}}$ (arcsec)	Env.	Note
(1)	(2)	(3)	(4)	(5)	(6)	(7)	(8)	(9)	(10)	(11)	(12)	(13)
NGC 0057	3.8787	17.3284	76.3	8.68	0.212	-25.75	326		13.2	27.0	1	
NGC 0080	5.2952	22.3572	81.9	8.92	0.168	-25.66	260		15.7	32.2	14 B	
NGC 0128	7.3128	2.8641	59.3	8.52	0.079	-25.35	215		10.5	18.0	1	
NGC 0227	10.6534	-1.5288	75.9	9.09	0.084	-25.32	262		8.7	27.2	4 B	
NGC 0315	14.4538	30.3524	70.3	7.96	0.177	-26.30	296		20.0	25.1	6 B	
NGC 0383	16.8540	32.4126	71.3	8.48	0.194	-25.81	279		15.5	20.5	29	=4ZW038
NGC 0393	17.1540	39.6443	85.7	9.23	0.120	-25.44	233		11.0		1	
NGC 0410	17.7453	33.1520	71.3	8.38	0.161	-25.90	298		16.8	31.6	29 B	
NGC 0467	19.7922	3.3008	75.8	9.01	0.092	-25.40	247		14.5	21.5	1	
PGC 004829	20.1287	50.1445	99.0	9.74	0.554	-25.30			7.3		1	
NGC 0499	20.7978	33.4601	69.8	8.74	0.193	-25.50	266		11.6	15.6	35	
NGC 0507	20.9164	33.2561	69.8	8.30	0.170	-25.93	295		23.0	38.4	35 B	
NGC 0533	21.3808	1.7590	77.9	8.42	0.084	-26.05	279		21.9	40.7	3 B	
NGC 0545 <sup>†</sup>	21.4963	-1.3402	74.0	0.114			250				32 B	A194
NGC 0547	21.5024	-1.3451	74.0	8.49	0.113	-25.83	262		25.1	19.7	32	A194
NGC 0665	26.2338	10.4230	74.6	8.88	0.242	-25.51	190		11.5	13.7	4 B	
UGC 01332	28.0755	48.0878	99.2	9.48	0.557	-25.57			12.9		8 B	
NGC 0708	28.1937	36.1518	69.0	8.57	0.247	-25.65	230		23.7		39 B	A262
UGC 01389	28.8778	47.9550	99.2	9.63	0.519	-25.41			9.2		8	
NGC 0741	29.0874	5.6289	73.9	8.30	0.144	-26.06	291		19.5	26.9	5 B	
NGC 0777	30.0622	31.4294	72.2	8.37	0.128	-25.94	318		14.6	18.6	7 B	
NGC 0890	35.5042	33.2661	55.6	8.25	0.212	-25.50	212		16.7		1	
NGC 0910	36.3616	41.8243	79.8	9.20	0.157	-25.33	249		13.6		29	A347
NGC 0997	39.3103	7.3056	90.4	9.42	0.380	-25.40			9.6	23.5	3 B	
NGC 1016	39.5815	2.1193	95.2	8.58	0.085	-26.33	302		18.1	26.8	8 B	
NGC 1060	40.8127	32.4250	67.4	8.20	0.532	-26.00	303		16.8	36.9	12 B	
NGC 1066	40.9579	32.4749	67.4	8.89	0.563	-25.31			17.5	26.6	12	
NGC 1132	43.2159	-1.2747	97.6	9.26	0.176	-25.70	246		16.1	30.9	3 B	
NGC 1129	43.6141	41.5796	73.9	8.24	0.309	-26.14	330		26.4	30.2	33 B	
NGC 1167	45.4265	35.2056	70.2	8.64	0.496	-25.64	204		20.7	29.7	3 B	
NGC 1226	47.7723	35.3868	85.7	9.21	0.526	-25.51	271		12.5		3 B	
IC 0310	49.1792	41.3248	77.5	9.15	0.445	-25.35	230	239	11.8	15.3	117	Perseus/A426
NGC 1272	49.8387	41.4906	77.5	8.69	0.441	-25.80	292		20.7	31.5	117	Perseus/A426
UGC 02783	53.5766	39.3568	85.8	9.27	0.447	-25.44	299		8.4	9.0	4 B	
NGC 1453	56.6136	-3.9688	56.4	8.12	0.289	-25.67	328		16.0		12 B	
NGC 1497	60.5283	23.1329	87.8	9.48	0.602	-25.31	249		10.3		1	
NGC 1600	67.9161	-5.0861	63.8	8.04	0.118	-25.99	334		20.8		16 B	
NGC 1573	68.7666	73.2624	65.0	8.56	0.377	-25.55	303		13.9		15 B	
NGC 1684	73.1298	-3.1061	63.5	8.69	0.159	-25.34	306		15.8		11 B	
NGC 1700	74.2347	-4.8658	54.4	8.09	0.119	-25.60	239		13.4		4 B	
NGC 2208	95.6444	51.9095	84.1	9.04	0.408	-25.63	225		14.2		1	
NGC 2256	101.8082	74.2365	79.4	8.67	0.359	-25.87	221		20.9		10 B	
NGC 2274	101.8224	33.5672	73.8	8.68	0.286	-25.69	295		15.0		6 B	
NGC 2258	101.9425	74.4818	59.0	8.23	0.351	-25.66	287		18.6		3 B	
NGC 2320	106.4251	50.5811	89.4	8.85	0.189	-25.93	315		10.6		18 B	
UGC 03683	107.0582	46.1159	85.1	9.16	0.253	-25.52	291		11.2		4 B	
NGC 2332	107.3924	50.1823	89.4	9.40	0.241	-25.39	232		8.9		18	
NGC 2340	107.7950	50.1747	89.4	8.88	0.203	-25.90	246		19.7		18	
UGC 03894	113.2695	65.0791	97.2	9.37	0.175	-25.58	304		12.2	17.8	4 B	
NGC 2418	114.1563	17.8839	74.1	8.95	0.102	-25.42	247		11.7	16.2	1	
NGC 2456	118.5444	55.4953	107.3	9.83	0.106	-25.33	214		10.9		1	
NGC 2492	119.8738	27.0264	97.8	9.60	0.109	-25.36	243	273	8.7	12.6	3 B	
NGC 2513	120.6028	9.4136	70.8	8.74	0.063	-25.52	274		13.9	24.0	4 B	
NGC 2672	132.3412	19.0750	61.5	8.35	0.058	-25.60	268		16.9	14.3	3 B	
NGC 2693	134.2469	51.3474	74.4	8.60	0.054	-25.76	349		13.7	15.4	1	
NGC 2783	138.4145	29.9929	101.4	9.32	0.082	-25.72	301	254	11.8	38.2	3 B	
NGC 2832	139.9453	33.7498	105.2	8.70	0.047	-26.42	332		18.2	21.2	4 B	A779
NGC 2892	143.2205	67.6174	101.1	9.35	0.233	-25.70	304		12.5	23.3	1	
NGC 2918	143.9334	31.7054	102.3	9.57	0.053	-25.49	258	223	8.8	18.9	1	
NGC 3158	153.4605	38.7649	103.4	8.80	0.036	-26.28	343	300	14.2	16.1	6 B	
NGC 3209	155.1601	25.5050	94.6	9.34	0.060	-25.55	303		9.0	29.4	3 B	
NGC 3332	160.1182	9.1825	89.1	9.37	0.087	-25.38	221	220	12.5	23.7	1	

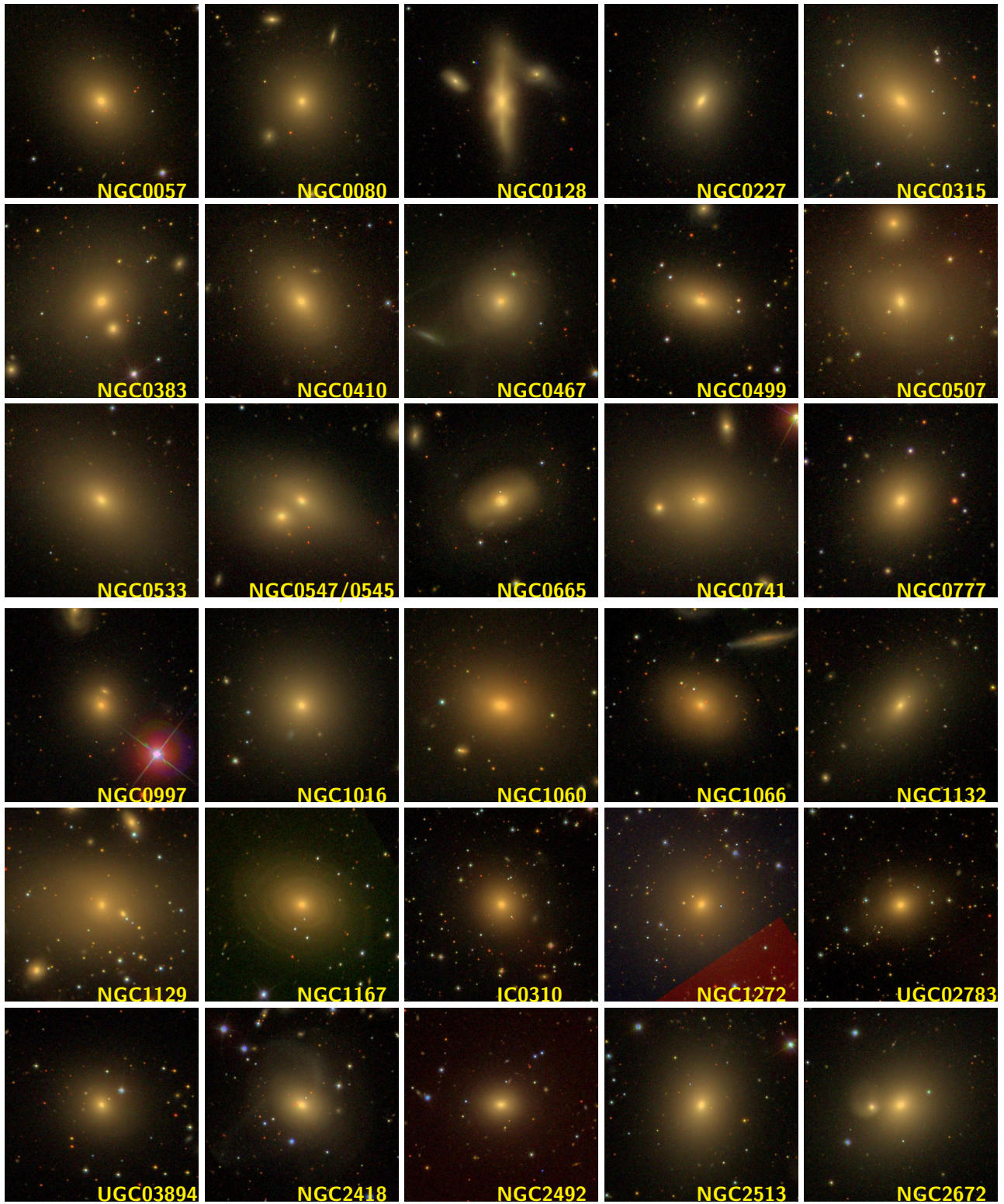
Table 3, continued

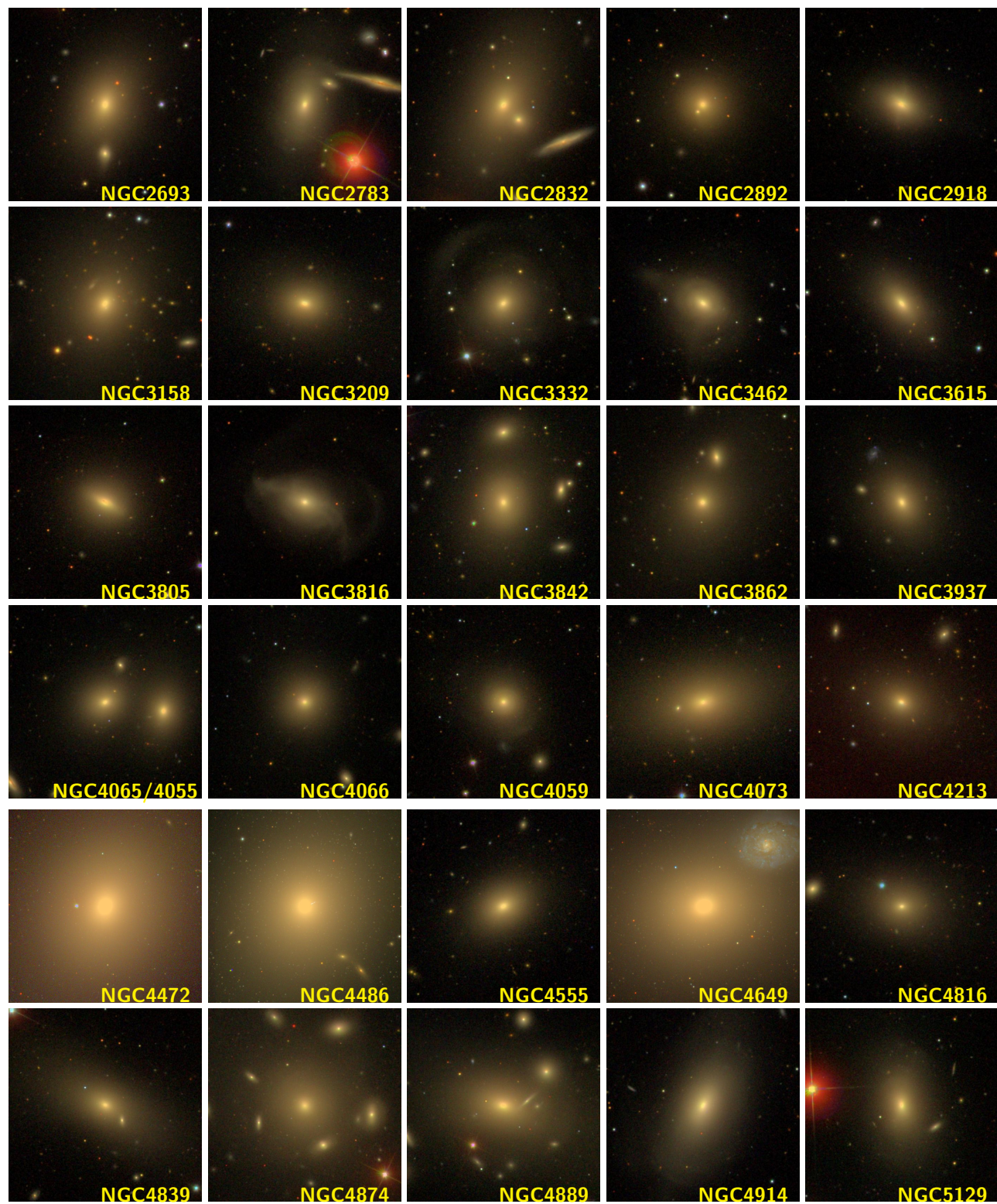
Galaxy	R.A.	Dec.	$D$	$K$	$A_V$	$M_K$	$\sigma^{\text{HL}}$	$\sigma^{\text{NSA}}$	$R_e^{2\text{MASS}}$	$R_e^{\text{NSA}}$	Env.	Note
(1)	(deg)	(deg)	(Mpc)	(mag)	(mag)	(mag)	(km/s)	(km/s)	(arcsec)	(arcsec)	(12)	(13)
NGC 3343	161.5432	73.3531	93.8	9.57	0.331	-25.33			10.6		1	
NGC 3462	163.8378	7.6967	99.2	9.37	0.081	-25.62	218		10.1	20.1	1	
NGC 3562	168.2445	72.8793	101.0	9.38	0.111	-25.65	264		8.6		3 B	
NGC 3615	169.5277	23.3973	101.2	9.45	0.049	-25.58	259	271	8.2	20.2	3 B	
NGC 3805	175.1736	20.3430	99.4	9.30	0.064	-25.69	293	295	8.3	16.5	42	
NGC 3816	175.4502	20.1036	99.4	9.60	0.052	-25.40	207	209	10.7	32.9	42	
NGC 3842	176.0090	19.9498	99.4	9.08	0.059	-25.91	315	291	14.1	24.2	42 B	A1367
NGC 3862	176.2708	19.6063	99.4	9.49	0.064	-25.50	271	260	11.1	40.0	42	
NGC 3937	178.1776	20.6313	101.2	9.42	0.117	-25.62	309	289	10.7	34.7	10 B	
NGC 4055	181.0059	20.2323	107.2	9.76	0.095	-25.40		270	8.1	17.5	18	=NGC 4061
NGC 4065	181.0257	20.2351	107.2	9.69	0.098	-25.47	272	283	8.8	31.0	18 B	
NGC 4066	181.0392	20.3479	107.2	9.81	0.086	-25.35		253	10.0	37.0	18	
NGC 4059	181.0471	20.4098	107.2	9.75	0.079	-25.41		206	9.6	33.0	18	
NGC 4073	181.1128	1.8960	91.5	8.49	0.074	-26.33	277	292	21.4	23.0	10 B	
NGC 4213	183.9064	23.9819	101.6	9.61	0.102	-25.44	259	264	11.6	33.6	4 B	
NGC 4472	187.4450	8.0004	16.7*	5.40	0.061	-25.72	289		53.9		205 B	=M49, Virgo
NGC 4486	187.7059	12.3911	16.7*	5.81	0.063	-25.31	336		41.3	48.7	205	=M87, Virgo
NGC 4555	188.9216	26.5230	103.6	9.17	0.044	-25.92	350	319	10.1	29.8	1	
NGC 4649	190.9167	11.5526	16.5*	5.74	0.072	-25.36	340		39.8	44.1	205	=M60, Virgo
NGC 4816	194.0506	27.7455	102.0*	9.71	0.024	-25.33	244		14.5	50.6	49	Coma/A1656
NGC 4839	194.3515	27.4977	102.0*	9.20	0.028	-25.85	285	269	20.8	29.2	49	Coma/A1656
NGC 4874	194.8988	27.9594	102.0*	8.86	0.025	-26.18	279	266	23.8	32.0	49	Coma/A1656
NGC 4889	195.0338	27.9770	102.0*	8.41	0.026	-26.64	401	370	19.1	33.0	49 B	Coma/A1656
NGC 4914	195.1789	37.3153	74.5	8.65	0.037	-25.72	225		12.8	31.3	1	=NGC 4912
NGC 5129	201.0417	13.9765	107.5	9.25	0.078	-25.92	277	262	12.3	21.8	1	
NGC 5208	203.1163	7.3166	105.0	9.51	0.097	-25.61		252	6.8	18.3	3 B	
PGC 047776	203.4770	3.2836	103.8	9.73	0.076	-25.36			7.9	13.2	9 B	
NGC 5252	204.5661	4.5426	103.8	9.77	0.095	-25.32	196		9.3	19.8	9	
NGC 5322	207.3133	60.1904	34.2	7.16	0.038	-25.51	236		26.6	20.1	8 B	
NGC 5353	208.3613	40.2831	41.1	7.63	0.035	-25.45	290		14.2	27.8	12 B	
NGC 5490	212.4888	17.5455	78.6	8.92	0.073	-25.57	288		10.1	19.5	1	
NGC 5557	214.6071	36.4936	51.0	8.08	0.016	-25.46	281		16.2	14.7	4 B	
IC 1143	232.7345	82.4558	97.3	9.51	0.172	-25.45			9.2		3 B	
UGC 10097	238.9303	47.8673	91.5	9.38	0.049	-25.43	302		7.6	17.2	7 B	
NGC 6223	250.7679	61.5789	86.7	9.11	0.100	-25.59			10.6		4 B	
NGC 6364	261.1139	29.3902	105.3	9.74	0.106	-25.38	205		7.7	11.5	1	
NGC 6375	262.3411	16.2067	95.8	9.42	0.334	-25.53	220		10.8		1	
UGC 10918	264.3892	11.1217	100.2	9.31	0.498	-25.75			12.8		1	
NGC 6442	266.7139	20.7611	98.0	9.59	0.239	-25.40	240		9.1		1	
NGC 6482	267.9534	23.0719	61.4	8.37	0.277	-25.60	322		10.1		3 B	
NGC 6575	272.7395	31.1162	106.0	9.56	0.172	-25.58	306		9.0		1	
NGC 7052	319.6377	26.4469	69.3	8.58	0.337	-25.67	284		14.7		1	
NGC 7242	333.9146	37.2987	84.4	8.33	0.415	-26.34			27.7		15 B	
NGC 7265	335.6145	36.2098	82.8	8.69	0.325	-25.93	258		16.0		21 B	
NGC 7274	336.0462	36.1259	82.8	9.24	0.295	-25.39	298		12.6		21	
NGC 7386	342.5089	11.6987	99.1	9.42	0.200	-25.58			11.6	38.1	3 B	
NGC 7426	344.0119	36.3614	80.0	8.82	0.337	-25.74			11.2		4 B	
NGC 7436	344.4897	26.1500	106.6	9.01	0.250	-26.16	352		19.1	25.0	8 B	
NGC 7550	348.8170	18.9614	72.7	8.91	0.375	-25.43	255		12.4	28.0	3 B	
NGC 7556	348.9353	-2.3815	103.0	9.25	0.097	-25.83	268		16.9	26.4	4 B	
NGC 7618	349.9468	42.8526	76.3	9.04	0.609	-25.44	298		9.8		10 B	
NGC 7619	350.0605	8.2063	54.0	8.03	0.224	-25.65	324		14.8	34.6	12 B	
NGC 7626	350.1772	8.2170	54.0	8.03	0.197	-25.65	274		20.1	26.7	12	
NGC 7681	352.2287	17.3096	96.8	9.22	0.149	-25.72	359		11.4	5.5	1	

Notes. Column (1): in order of increasing R.A. Column (2): right ascension in degrees (J2000.0). Column (3): declination in degrees (J2000.0). Column (4): distance. Symbol \* indicates SBF distances; others are from group-corrected flow velocities, as described in Sec 2.2. Column (5): “total” galaxy apparent  $K$ -band magnitude from 2MASS XSC (parameter  $k\_m\_ext$ ). Column (6): foreground galactic extinction in Landolt  $V$ -band (Schlafly & Finkbeiner 2011) with reddening relation of Fitzpatrick (1999). Column (7): extinction-corrected “total” absolute  $K$ -band magnitude derived from distance in column (4), apparent magnitude in column (5), and foreground extinction in column (6), using Equation (1). Column (8): central stellar velocity dispersion from HyperLeda. Column (9): central stellar velocity dispersion from the NASA-Sloan Atlas. Column (10): effective radius from 2MASS, defined in Equation (3). Column (11): optical half-light radius from the NASA-Sloan Atlas. Column (12): galaxy environment – number of group members in the 2MASS HDC group catalog (Crook et al. 2007); “B” indicates brightest group galaxy. Column (13): additional comments, e.g., alternative names, associated clusters.

† NGC 545 is a close companion of NGC 547. It is not listed in 2MASS but is designated the BCG of Abell 194 with  $M_V = -22.98$  in Lauer et al. (2007b).







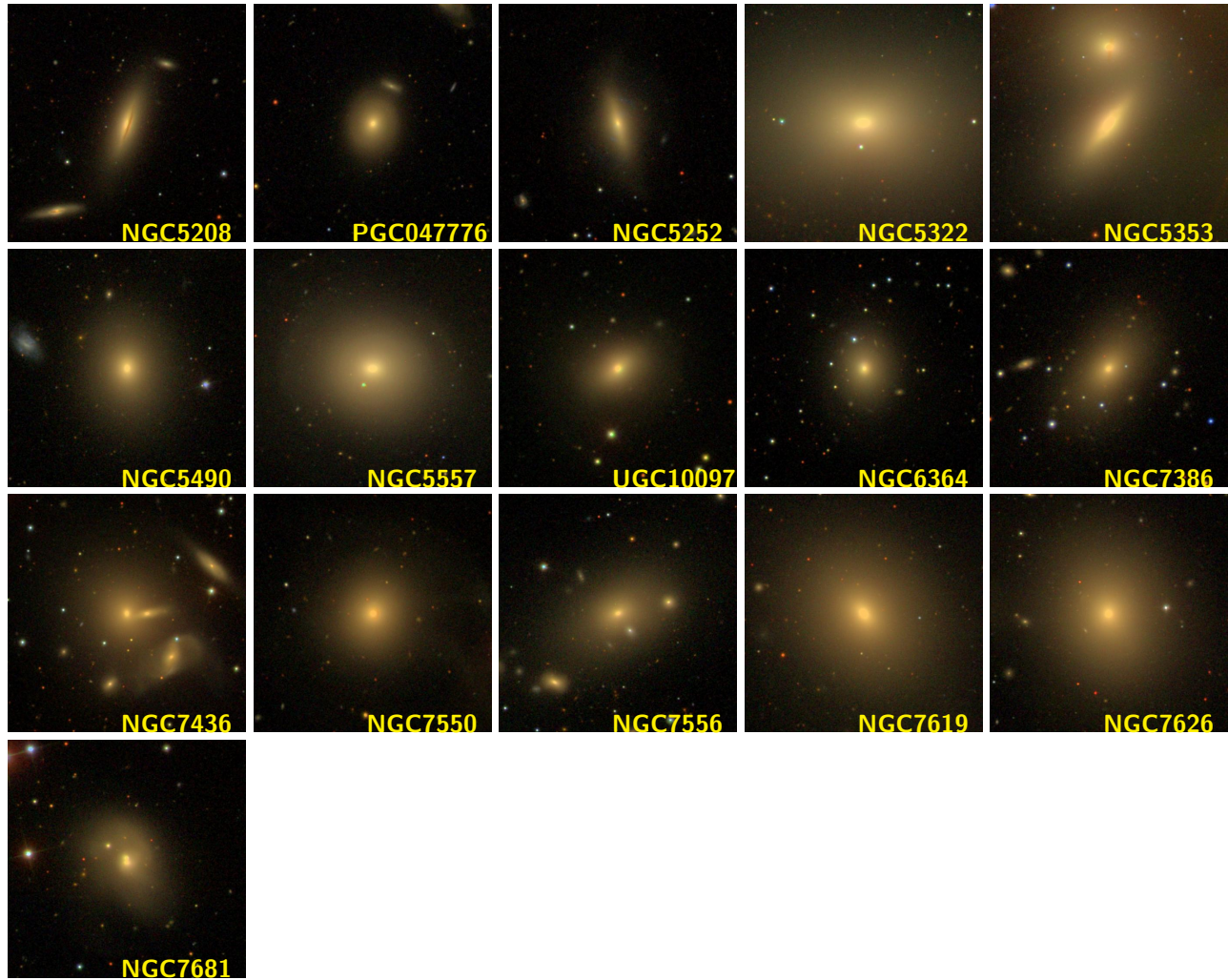


FIG. 14.— Red-blue-green composite images of SDSS photometry for 78 MASSIVE galaxies. The rest of the sample is not in the SDSS footprint. Each postage stamp shows a  $220'' \times 220''$  field of view. The three exceptions are the Virgo galaxies NGC 4472, NGC 4486, and NGC 4649, which are zoomed out to  $340'' \times 340''$ . We note that NGC 4472 was in SDSS but not in NSA.

## REFERENCES

- Adams, J. J., Gebhardt, K., Blanc, G. A., et al. 2012, *ApJ*, 745, 92
- Adams, J. J., et al. 2011, *ApJS*, 192, 5
- Aihara, H., et al. 2011, *ApJS*, 193, 29
- Allen, S. W., Dunn, R. J. H., Fabian, A. C., Taylor, G. B., & Reynolds, C. S. 2006, *MNRAS*, 372, 21
- Anglés-Alcázar, D., Özel, F., & Davé, R. 2013, *ApJ*, 770, 5
- Arnold, J. A., Romanowsky, A. J., Brodie, J. P., et al. 2014, *ApJ*, 791, 80
- Auger, M. W., Treu, T., Gavazzi, R., et al. 2010, *ApJ*, 721, L163
- Barden, S. C., Sawyer, D. G., & Honeycutt, R. K. 1998, in *Society of Photo-Optical Instrumentation Engineers (SPIE) Conference Series*, Vol. 3355, *Society of Photo-Optical Instrumentation Engineers (SPIE) Conference Series*, ed. S. D’Odorico, 892–899
- Barnabè, M., Czoske, O., Koopmans, L. V. E., Treu, T., & Bolton, A. S. 2011, *MNRAS*, 415, 2215
- Barnabè, M., Spiniello, C., Koopmans, L. V. E., et al. 2013, *MNRAS*, 436, 253
- Begelman, M. C., Blandford, R. D., & Rees, M. J. 1980, *Nature*, 287, 307
- Beifiori, A., Courteau, S., Corsini, E. M., & Zhu, Y. 2012, *MNRAS*, 419, 2497
- Bender, R., Surma, P., Doebereiner, S., Moellenhoff, C., & Madejsky, R. 1989, *A&A*, 217, 35
- Bernardi, M., Meert, A., Vikram, V., et al. 2012, *ArXiv e-prints*
- Bernardi, M., Sheth, R. K., Annis, J., et al. 2003a, *AJ*, 125, 1866
- . 2003b, *AJ*, 125, 1882
- Binney, J. 1978, *MNRAS*, 183, 501
- Blakeslee, J. P. 2013, in *IAU Symposium*, Vol. 289, *IAU Symposium*, ed. R. de Grijs, 304–311
- Blakeslee, J. P., Franx, M., Postman, M., et al. 2003, *ApJ*, 596, L143
- Blakeslee, J. P., Jordán, A., Mei, S., et al. 2009, *ApJ*, 694, 556
- Blakeslee, J. P., Cantiello, M., Mei, S., et al. 2010, *ApJ*, 724, 657
- Blanc, G. A., Heiderman, A., Gebhardt, K., Evans, II, N. J., & Adams, J. 2009, *ApJ*, 704, 842
- Blanc, G. A., Weinzirl, T., Song, M., et al. 2013, *AJ*, 145, 138

- Blanton, M. R., Eisenstein, D., Hogg, D. W., Schlegel, D. J., & Brinkmann, J. 2005, *ApJ*, 629, 143
- Blanton, M. R., Kazin, E., Muna, D., Weaver, B. A., & Price-Whelan, A. 2011, *AJ*, 142, 31
- Bolton, A. S., Schlegel, D. J., Aubourg, É., et al. 2012, *AJ*, 144, 144
- Bower, R. G., Lucey, J. R., & Ellis, R. S. 1992, *MNRAS*, 254, 601
- Boylan-Kolchin, M., Ma, C.-P., & Quataert, E. 2005, *MNRAS*, 362, 184
- . 2006, *MNRAS*, 369, 1081
- Brodie, J. P., Romanowsky, A. J., Strader, J., et al. 2014, *ArXiv e-prints*
- Canning, R. E. A., Ryon, J. E., Gallagher, J. S., et al. 2014, *MNRAS*, 444, 336
- Cantiello, M., Blakeslee, J., Raimondo, G., Brocato, E., & Capaccioli, M. 2007, *ApJ*, 668, 130
- Cappellari, M. 2013, *ApJ*, 778, L2
- Cappellari, M., & Emsellem, E. 2004, *PASP*, 116, 138
- Cappellari, M., di Serego Alighieri, S., Cimatti, A., et al. 2009, *ApJ*, 704, L34
- Cappellari, M., et al. 2011, *MNRAS*, 413, 813
- . 2012, *Nature*, 484, 485
- Carollo, C. M., & Danziger, I. J. 1994, *MNRAS*, 270, 523
- Conroy, C., & van Dokkum, P. 2012, *ApJ*, 747, 69
- Crook, A. C., Huchra, J. P., Martimbeau, N., et al. 2007, *ApJ*, 655, 790
- . 2008, *ApJ*, 685, 1320
- Croom, S. M., Lawrence, J. S., Bland-Hawthorn, J., et al. 2012, *MNRAS*, 421, 872
- Daddi, E., et al. 2005, *ApJ*, 626, 680
- Damjanov, I., et al. 2009, *ApJ*, 695, 101
- Davies, R. L., Efstathiou, G., Fall, S. M., Illingworth, G., & Schechter, P. L. 1983, *ApJ*, 266, 41
- De Lucia, G., Springel, V., White, S. D. M., Croton, D., & Kauffmann, G. 2006, *MNRAS*, 366, 499
- de Vaucouleurs, G., de Vaucouleurs, A., Corwin, Jr., H. G., et al. 1991, *Third Reference Catalogue of Bright Galaxies. Volume I: Explanations and references. Volume II: Data for galaxies between 0<sup>h</sup> and 12<sup>h</sup>. Volume III: Data for galaxies between 12<sup>h</sup> and 24<sup>h</sup>.*
- Demorest, P. B., Ferdman, R. D., Gonzalez, M. E., et al. 2013, *ApJ*, 762, 94
- Desroches, L.-B., Quataert, E., Ma, C.-P., & West, A. A. 2007, *MNRAS*, 377, 402
- Diehl, S., & Statler, T. S. 2008, *ApJ*, 680, 897
- Donato, D., Sambruna, R. M., & Gliozzi, M. 2004, *ApJ*, 617, 915
- Dressler, A., Lynden-Bell, D., Burstein, D., et al. 1987, *ApJ*, 313, 42
- Dunn, R. J. H., Allen, S. W., Taylor, G. B., et al. 2010, *MNRAS*, 404, 180
- Dutton, A. A., Macciò, A. V., Mendel, J. T., & Simard, L. 2013, *MNRAS*, 432, 2496
- Eisenhardt, P. R., De Propris, R., Gonzalez, A. H., et al. 2007, *ApJS*, 169, 225
- Emsellem, E., Monnet, G., & Bacon, R. 1994, *A&A*, 285, 723
- Emsellem, E., Cappellari, M., Krajnović, D., et al. 2011, *MNRAS*, 414, 888
- Fabbiano, G. 1989, *ARA&A*, 27, 87
- Faber, S. M., Friel, E. D., Burstein, D., & Gaskell, C. M. 1985, *ApJS*, 57, 711
- Faber, S. M., & Jackson, R. E. 1976, *ApJ*, 204, 668
- Faber, S. M., et al. 1997, *AJ*, 114, 1771
- Faber, S. M., Willmer, C. N. A., Wolf, C., et al. 2007, *ApJ*, 665, 265
- Ferrarese, L., & Merritt, D. 2000, *ApJ*, 539, L9
- Ferrarese, L., Côté, P., Jordán, A., et al. 2006, *ApJS*, 164, 334
- Fitzpatrick, E. L. 1999, *PASP*, 111, 63
- Forman, W., Jones, C., & Tucker, W. 1985, *ApJ*, 293, 102
- Franx, M., Illingworth, G., & de Zeeuw, T. 1991, *ApJ*, 383, 112
- Gebhardt, K., Adams, J., Richstone, D., et al. 2011, *ApJ*, 729, 119
- Gebhardt, K., & Thomas, J. 2009, *ApJ*, 700, 1690
- Gebhardt, K., Richstone, D., Kormendy, J., et al. 2000, *AJ*, 119, 1157
- Graves, G. J., Faber, S. M., & Schiavon, R. P. 2009, *ApJ*, 693, 486
- Graves, G. J., Faber, S. M., Schiavon, R. P., & Yan, R. 2007, *ApJ*, 671, 243
- Graves, G. J., & Schiavon, R. P. 2008, *ApJS*, 177, 446
- Greene, J. E., Murphy, J. D., Comerford, J. M., Gebhardt, K., & Adams, J. J. 2012, *ApJ*, 750, 32
- Greene, J. E., Murphy, J. D., Graves, G. J., et al. 2013, *ApJ*, 776, 64
- Greene, J. E., Peng, C. Y., Kim, M., et al. 2010, *ApJ*, 721, 26
- Gültekin, K., et al. 2009, *ApJ*, 698, 198
- Häring, N., & Rix, H.-W. 2004, *ApJ*, 604, L89
- Heisler, J., Tremaine, S., & Bahcall, J. N. 1985, *ApJ*, 298, 8
- Hill, G. J., et al. 2008, in *Society of Photo-Optical Instrumentation Engineers (SPIE) Conference Series*, Vol. 7014, *Society of Photo-Optical Instrumentation Engineers (SPIE) Conference Series*
- Hilz, M., Naab, T., & Ostriker, J. P. 2013, *MNRAS*, 429, 2924
- Hirschmann, M., Khochfar, S., Burkert, A., et al. 2010, *MNRAS*, 407, 1016
- Ho, L. C. 2007, *ApJ*, 668, 94
- Huchra, J. P., et al. 2012, *ApJS*, 199, 26
- Jahnke, K., & Macciò, A. V. 2011, *ApJ*, 734, 92
- Jarrett, T. H., Chester, T., Cutri, R., et al. 2000, *AJ*, 119, 2498
- Jarrett, T. H., Chester, T., Cutri, R., Schneider, S. E., & Huchra, J. P. 2003, *AJ*, 125, 525
- Jones, L. R., Ponman, T. J., Horton, A., et al. 2003, *MNRAS*, 343, 627
- Kelson, D. D., Illingworth, G. D., Franx, M., & van Dokkum, P. G. 2006, *ApJ*, 653, 159
- Kim, D.-W., & Fabbiano, G. 2013, *ApJ*, 776, 116
- Kormendy, J. 1977, *ApJ*, 218, 333
- Kormendy, J., & Bender, R. 1996, *ApJ*, 464, L119
- . 2009, *ApJ*, 691, L142
- Kormendy, J., Fisher, D. B., Cornell, M. E., & Bender, R. 2009, *ApJS*, 182, 216
- Kormendy, J., & Ho, L. C. 2013, *ARA&A*, 51, 511
- Krajnović, D., Emsellem, E., Cappellari, M., et al. 2011, *MNRAS*, 414, 2923
- Krajnović, D., Karick, A. M., Davies, R. L., et al. 2013, *MNRAS*, 433, 2812
- Kuo, C. Y., et al. 2011, *ApJ*, 727, 20
- Larkin, J., Barczys, M., Krabbe, A., et al. 2006, in *Society of Photo-Optical Instrumentation Engineers (SPIE) Conference Series*, Vol. 6269, *Society of Photo-Optical Instrumentation Engineers (SPIE) Conference Series*
- Läsker, R., Ferrarese, L., & van de Ven, G. 2014, *ApJ*, 780, 69
- Lauer, T. R., Tremaine, S., Richstone, D., & Faber, S. M. 2007a, *ApJ*, 670, 249
- Lauer, T. R., et al. 2007b, *ApJ*, 662, 808
- Lavaux, G., & Hudson, M. J. 2011, *MNRAS*, 416, 2840
- Magorrian, J., Tremaine, S., Richstone, D., et al. 1998, *AJ*, 115, 2285
- Marconi, A., & Hunt, L. K. 2003, *ApJ*, 589, L21
- Martin-Navarro, I., La Barbera, F., Vazdekis, A., Falcón-Barroso, J., & Ferreras, I. 2014, *MNRAS*, submitted (arXiv:1404.6533)
- Mathews, W. G., Brighenti, F., Faltenbacher, A., et al. 2006, *ApJ*, 652, L17
- McConnell, N. J., & Ma, C.-P. 2013, *ApJ*, 764, 184
- McConnell, N. J., Ma, C.-P., Gebhardt, K., et al. 2011a, *Nature*, 480, 215
- McConnell, N. J., Ma, C.-P., Graham, J. R., et al. 2011b, *ApJ*, 728, 100
- McConnell, N. J., Ma, C.-P., Murphy, J. D., et al. 2012, *ApJ*, 756, 179
- McNamara, B. R., & Nulsen, P. E. J. 2007, *ARA&A*, 45, 117
- Mehlert, D., Thomas, D., Saglia, R. P., Bender, R., & Wegner, G. 2003, *A&A*, 407, 423
- Memola, E., Trinchieri, G., Wolter, A., Focardi, P., & Kelm, B. 2009, *A&A*, 497, 359
- Mould, J. R., Huchra, J. P., Freedman, W. L., et al. 2000, *ApJ*, 529, 786
- Mulchaey, J. S., & Jeltema, T. E. 2010, *ApJ*, 715, L1
- Murphy, J. D., Gebhardt, K., & Adams, J. J. 2011, *ApJ*, 729, 129
- Naab, T., Johansson, P. H., & Ostriker, J. P. 2009, *ApJ*, 699, L178
- Naab, T., Johansson, P. H., Ostriker, J. P., & Efstathiou, G. 2007, *ApJ*, 658, 710
- Naab, T., Oser, L., Emsellem, E., et al. 2014, *MNRAS*, 444, 3357
- Oguri, M., Rusu, C. E., & Falco, E. E. 2014, *MNRAS*, 439, 2494

- Oser, L., Ostriker, J. P., Naab, T., Johansson, P. H., & Burkert, A. 2010, *ApJ*, 725, 2312
- O'Sullivan, E., & Ponman, T. J. 2004, *MNRAS*, 354, 935
- O'Sullivan, E., Sanderson, A. J. R., & Ponman, T. J. 2007, *MNRAS*, 380, 1409
- Pastorello, N., Forbes, D. A., Foster, C., et al. 2014, *MNRAS*, 442, 1003
- Paturel, G., Petit, C., Prugniel, P., et al. 2003, *A&A*, 412, 45
- Peng, C. Y. 2007, *ApJ*, 671, 1098
- Ponman, T. J., Allan, D. J., Jones, L. R., et al. 1994, *Nature*, 369, 462
- Prugniel, P., & Simien, F. 1996, *A&A*, 309, 749
- Pu, S. B., Saglia, R. P., Fabricius, M. H., et al. 2010, *A&A*, 516, A4
- Raskutti, S., Greene, J. E., & Murphy, J. D. 2014, *ApJ*, 786, 23
- Robertson, B., et al. 2006, *ApJ*, 641, 21
- Rusli, S. P., Erwin, P., Saglia, R. P., et al. 2013a, *AJ*, 146, 160
- Rusli, S. P., Thomas, J., Erwin, P., et al. 2011, *MNRAS*, 410, 1223
- Rusli, S. P., Thomas, J., Saglia, R. P., et al. 2013b, *AJ*, 146, 45
- Sánchez, S. F., Kennicutt, R. C., Gil de Paz, A., et al. 2012, *A&A*, 538, A8
- Sánchez-Blázquez, P., Peletier, R. F., Jiménez-Vicente, J., et al. 2006, *MNRAS*, 371, 703
- Schlafly, E. F., & Finkbeiner, D. P. 2011, *ApJ*, 737, 103
- Schombert, J., & Smith, A. K. 2012, *PASA*, 29, 174
- Schulze, A., & Gebhardt, K. 2011, *ApJ*, 729, 21
- Shannon, R. M., Ravi, V., Coles, W. A., et al. 2013, *Science*, 342, 334
- Shen, J., & Gebhardt, K. 2010, *ApJ*, 711, 484
- Skrutskie, M. F., Cutri, R. M., Stiening, R., et al. 2006, *AJ*, 131, 1163
- Smith, R. J. 2014, *MNRAS*, 443, L69
- Smith, R. J., & Lucey, J. R. 2013, *MNRAS*, 434, 1964
- Sonnenfeld, A., et al. 2012, *ApJ*, 752, 163
- Spiniello, C., Trager, S., Koopmans, L. V. E., & Conroy, C. 2014, *MNRAS*, 438, 1483
- Spolaor, M., Kobayashi, C., Forbes, D. A., Couch, W. J., & Hau, G. K. T. 2010, *MNRAS*, 408, 272
- Sun, A.-L., Greene, J. E., Impellizzeri, C. M. V., et al. 2013, *ApJ*, 778, 47
- Thomas, D., Maraston, C., Bender, R., & Mendes de Oliveira, C. 2005, *ApJ*, 621, 673
- Thomas, J., Saglia, R. P., Bender, R., Erwin, P., & Fabricius, M. 2014, *ApJ*, 782, 39
- Thomas, J., et al. 2007, *MNRAS*, 382, 657
- Thomas, J., Saglia, R. P., Bender, R., et al. 2011, *MNRAS*, 415, 545
- Tortora, C., Romanowsky, A. J., & Napolitano, N. R. 2013, *ApJ*, 765, 8
- Tremaine, S., et al. 2002, *ApJ*, 574, 740
- Tremblay, B., & Merritt, D. 1996, *AJ*, 111, 2243
- Treu, T., Auger, M. W., Koopmans, L. V. E., et al. 2010, *ApJ*, 709, 1195
- Trujillo, I., et al. 2006, *MNRAS*, 373, L36
- van de Sande, J., Kriek, M., Franx, M., et al. 2011, *ApJ*, 736, L9
- van den Bosch, R. C. E., Gebhardt, K., Gültekin, K., et al. 2012, *Nature*, 491, 729
- van der Marel, R. P., & van den Bosch, F. C. 1998, *AJ*, 116, 2220
- van der Wel, A., Holden, B. P., Zirm, A. W., et al. 2008, *ApJ*, 688, 48
- van Dokkum, P. G., et al. 2008, *ApJ*, 677, L5
- . 2010, *ApJ*, 709, 1018
- van Haasteren, R., Levin, Y., Janssen, G. H., et al. 2011, *MNRAS*, 414, 3117
- Walcher, C. J., Wisotzki, L., Bekeraité, S., et al. 2014, *A&A*, 569, A1
- Walsh, J. L., Barth, A. J., Ho, L. C., & Sarzi, M. 2013, *ApJ*, 770, 86
- Wegner, G. A., Corsini, E. M., Thomas, J., et al. 2012, *AJ*, 144, 78
- Weijmans, A.-M., et al. 2009, *MNRAS*, 398, 561
- Worthey, G., Faber, S. M., Gonzalez, J. J., & Burstein, D. 1994, *ApJS*, 94, 687
- Wu, X., Gerhard, O., Naab, T., et al. 2014, *MNRAS*, 438, 2701
- York, D. G., Adelman, J., Anderson, Jr., J. E., et al. 2000, *AJ*, 120, 1579